Laser shock peening without coating induced residual stress distribution, wettability characteristics and enhanced pitting corrosion resistance of austenitic stainless steel

Prabhakaran , S, Kulkarni , A, Vasanth, G, Kalainathan , S, Shukla, P & Vasudevan , V

Original citation & hyperlink:
Prabhakaran , S, Kulkarni , A, Vasanth, G, Kalainathan , S, Shukla, P & Vasudevan , V 2017, 'Laser shock peening without coating induced residual stress distribution, wettability characteristics and enhanced pitting corrosion resistance of austenitic stainless steel' *Applied Surface Science*, vol 428, pp. 17 - 30
https://dx.doi.org/10.1016/j.apsusc.2017.09.138

DOI 10.1016/j.apsusc.2017.09.138
ISSN 0169-4332

Publisher: Elsevier

Laser shock peening without coating induced residual stress distribution, wettability characteristics and enhanced pitting corrosion resistance of austenitic stainless steel

S. Prabhakaran [a,b], Aniket Kulkarni [a,b], G. Vasanth [b], S. Kalainathan [a]*, Pratik Shukla [c], Vijay K. Vasudevan [d]

[a] *Centre for Crystal Growth, VIT University, Vellore - 632 014, Tamilnadu, India*

[b] *Department of Physics, School of Advanced Sciences, VIT University, Vellore - 632 014, Tamilnadu, India*

[c] *School of Mechanical, Aerospace and Automotive Engineering, Coventry University, Priory Street, Coventry, CV1 5FB, United Kingdom*

[d] *Department of Mechanical and Materials Engineering, University of Cincinnati, OH 45221-0072, United States*

***Corresponding author E-mail: kalainathan@yahoo.com (S. Kalainathan);**

First-author E-mail: spkaran.kmd@gmail.com (S. Prabhakaran)

Abstract

Low energy laser shock peening without coating (LSPwC) was conducted on AISI 304 austenitic stainless steel specimens with varying pulse densities or overlapping. Highest magnitude of compressive residual stress (CRS) was achieved for an optimized pulse density of 2500 pulses/cm^2 (75% overlapping). The 2-D and 3-D topographical analysis were indicative of the fact that controlled roughening of the surface was achieved after the LSPwC process. After the LSPwC process, the hydrophilic unpeened surface was converted into the hydrophobic surface, thus decreasing the wettability characteristics of the surface. The X-ray diffraction (XRD) results reveal that there is a beginning of the martensite transformation and the rise in the intensity value of the peaks after LSPwC indicates the presence of compressive residual stresses induced in the specimen. The optical microscope and high-resolution transmission electron microscope results provided evidence of grain refinement and deformation induced refinement features such as multidirectional mechanical twinning, dislocations lines, micro shear cells and stacking faults in the near and sub-surface areas. The average hardness value of the LSPwC specimens was found to be increased by 28% more than the untreated specimen. The potentiodynamic polarization revealed that there was a considerable amount of increase in the pitting corrosion resistance after the LSPwC process, thus, supporting to extend the fatigue life of the specimen. The electrochemical impedance spectroscopic (EIS) analysis depicts that the LSPwC process supports the formation of the strong passivation layer in 3.5% NaCl solution.

Keywords: *Laser shock peening without coating (LSPwC); Residual Stress; Wettability; Grain refinement; Pitting Corrosion*

1. Introduction

Varieties of stainless steels are used in nuclear reactors, marine applications, biomedical implant applications, food industries, jewelry and other engineering applications [1]. Especially in nuclear reactors, metals used in reactor cores need to perform optimally in at elevated temperature range of 300-350 °C as well as in aqueous environments. The conditions inside a nuclear reactor may lead to corrosion or stress corrosion cracking (SCC), radiation hardening [2], radiation defects and radiation embrittlement or helium embrittlement of the metals. Therefore it is essential and advisable to use materials which can withstand those conditions. In nuclear fission reactors, especially AISI 304 austenitic stainless steel is used as core and pump structural parts, primary piping, preheater tubing and in steam dryers [3-5]. For the biomedical applications, the surface conditions such as wettability characteristics and corrosion resistance of the implants are crucial for the cell adhesion and proliferations [1,6-8].

Laser shock peening without coating (LSPwC) using low energy laser on SUS 304 and 316L austenitic stainless steel as revealed by Sano and Kalainathan *et al*. [6,7]. Sano *et al*. [6] utilized the second harmonic laser for underwater nuclear power plant maintenance applications, and their research explained that LSPwC could induce compressive residual stress on the surface and prompts to the aversion of SCC start and enhancement of fatigue strength. Q. Lu *et al*. [2] performed laser shock peening (LSP) on 304 austenitic stainless steel and unveiled that the dislocation sinks created due to LSP process help in improving radiation resistance and lowering the radiation defect densities at room temperature (25 °C) and as well as at 300 °C. Peyre *et al*. [8] carried out LSP on 316L austenitic stainless steel and revealed the post beneficial effects of LSP on its pitting corrosion resistance. LSPwC was performed on AISI 304 austenitic stainless steel, and it can viably hinder crack initiation and development in austenitic stainless steels as it

converted the surface tensile residual stress to the compressive residual stress of hundreds of MPa by Sano *et al*. [6]. It was revealed previously that creation of dislocations and deformation of the crystal lattice are responsible for enhancing the mechanical properties and fatigue life of austenitic stainless steels [1, 8].

In most of the materials, fatigue cracks commence at the surface of the material and then propagate through the entire material which ultimately leads to fatigue fracture. Therefore in order to prevent this from occurring we utilize surface modification techniques. Different methods of surface modification techniques namely: shot peening (SP), cold rolling, ball milling, surface mechanical attrition treatment (SMAT), ultrasonic peening and laser shock peening (LSP), have been produced to considerably refine the grains in metals and its alloys keeping in mind the end goal to improve their surface properties [9-12]. LSP is a cold working process that could actuate compressive residual stresses through various progressive and controlled impacts of a pulsed laser beam [6]. LSP is superior to existing shot peening technique in terms of inducing high magnitude of compressive residual stress while maintaining low surface roughness at the same time [8]. Dai *et.al* has reported the controlled surface roughness induction through LSP by tuning laser pulse overlapping or pulse density technique [13]. LSP process has the capability of improving the microstructural properties of the material, thus, enhancing its performance [14,15]. It is one of the most novel and innovative methods used for surface engineering. Whereby, - the compressive residual stresses are instigated amid the LSP process. This successfully hinders the fatigue crack initiation and proliferation. The shock waves which are produced due to laser ablation induced high-pressure plasma, additionally induce pressure at the surface and furthermore at a subsurface of the material [14,16]. When the initiated shock

pressure increments higher than the dynamic yield strength of the treated material (also called as Hugoniot Elastic Limit) given by the equation,

$$HEL = \frac{1-\nu}{1-2\nu}\sigma_y^{dyn} \quad \ldots (1)$$

Where the dynamic yield strength is σ_y^{dyn}, and the Poisson's ratio is 'υ'. [12] A plastic deformation and compressive stress induced in the surface and subsurface layer of the workpiece. It was observed that when the laser came in contact with the specimen surface, the surface was instantly transformed into greyish appearance. It is very much related with the past reports, and its cause can be justified as the reaction of the surface with nascent-state oxygen provided from the water decay by dynamic plasma and the extreme electric field of the laser [6, 18]. This may be the purpose behind the sudden change in the appearance. From direct perception, it was comprehended that as the pulse density has increased the surface lost its reflectivity and showed up as darker [6, 19]. Also, the surface roughness plays an important factor in deciding the wettability characteristics of the metallic materials [20].

The essential procedure of LSP without protective coating is outlined in **Fig. 1.** At the point when a laser pulse with a span of a few nanoseconds is centred on a metallic material, the surface begins to ablate immediately. The laser processing parameters control the metal surface layer removal during the ablation and, the subsequent high-density metal vapor is instantly transmuted to form high energy plasma plumes [6]. When the upcoming laser energy is taken up by the plasma, a heat enduring shock wave is created which encroaches on the material with a power of a few GPa, far surpassing the yield strength of the standard material [6,21]. The shock wave proliferates and loses energy as it spreads, and the material is deformed permanently [6,22,23]. After the shock wave has proliferated, the strained area is elastically compelled to

induce compressive residual stress at the surface [6]. The highest attainable strength of the material is determined by its resistance to crack initiation. The damage tolerance capacity of the material is exhibited by its fracture toughness and describes the loading states under which cracks proliferate [12,16,23].

The goal of the present work is to enhance the surface mechanical and corrosion properties of AISI 304 austenitic stainless steel by an advanced laser shock peening process and to explore the resulting residual stress dissemination and its correlation to lattice strain, microstructure, surface roughness and topography along with microhardness. The effect of the LSPwC process on contact angle and electrochemical behavior has also been elucidated. The contact angle greatly depends on the surface roughness, surface free energy and chemical composition of the element [20,24].

2. Experiments and methods

2.1 Metallic Sample Preparation

The AISI 304 austenitic stainless steel specimen was cut into square shape with dimensions of 10 mm x 10 mm x 5 mm using an electrical discharge machining (EDM). The chemical composition of the as-received sample was obtained using the optical emission spectrometric method. ARL Quantris Spark Analyzer (Thermo Electron, SWISS) was the instrument used in this method. The solution annealing was carried out in a tubular vacuum furnace at 1060℃ for duration of 30 minutes, trailed by sudden quenching with water. In order to relieve the internal stresses generated during quenching it was later kept at 400℃ for duration of 60 minutes. In prior to LSPwC process, the samples were ground using SiC abrasive wheels with varying roughness grades (220-3000) and polished with velvet cloth using diamond paste of 0.5

microns in order to ensure that LSP was done on a flat and original surface. The table 1 and 2 display the chemical composition and mechanical properties of AISI 304 austenitic stainless steel respectively.

Table-1 Nominal chemical composition of AISI 304 austenitic stainless steel

C	Zn	Si	Mn	P	S	Ni	Cr	Mo	V	Cu	W	Mg
0.065	0.018	0.64	0.91	0.027	0.002	8.24	18.32	0.41	0.097	0.29	0.013	0.006
Ti	Ce	Sn	Co	Al	Pb	B	Sb	Nb	Zr	Bi	Ca	Fe
0.012	0.002	0.016	0.15	0.007	0.008	0.002	0.083	0.06	0.008	0.059	0.0003	70.36

All values are in % wt.

Table-2a Mechanical properties of AISI 304 austenitic stainless steel

Property	Value
Ultimate tensile strength (σ_b)	505 MPa
Yield strength (σ)	215 MPa
Elongation (δ)	70 (%)
Modulus of Elasticity (E)	193-200 (GPa)
Poisson's ratio	0.29
HEL	1.5 GPa

2.2 Laser shock peening without coating

Table-2b Applied laser processing parameters for AISI 304 austenitic stainless steel

Laser parameter	Value
Pulse energy	400 mJ
Pulse duration	10 ns
Power density	8 $GWcm^{-2}$
Spot diameter	0.8 mm
Repetition rate	10 Hz
Radiance density	345.04 mW cm^2 Sr^{-1} µm
Overlapping (optimized)	75%

A Q-switched Nd: YAG laser (LPY704G-10, Litron Lasers Ltd., Rugby, UK) operating at the wavelength of 1064 nm was used in the LSPwC process. The laser comprised of an M^2 (beam quality factor) value of 2 and a beam divergence of 0.8 mrad. The beam shape was a top hat profile, and a $TEM_{00,}$ therefore, the exhibited radiance density (laser beam brightness) was 345.04 mW cm^2 Sr^{-1}.µm, as determined by the methodology from our previous work [21] as stated in Table-2b. There was no sacrificial coating utilized during the LSP process. Hence the name without coating was added to LSP. The experiment was performed at room temperature (25℃) [23]. **Fig.1** illustrates a schematic diagram of the LSPwC setup. The laser beam was delivered to the material surface with the help of a dichromatic mirror and a bi-convex lens of focal length 300 mm [18]. The dichromatic mirror was kept at an angle of 45˚ and after that the bi-convex lens was placed as shown in **Fig.1.** The lens is protected from the water spilling during

the time of laser peening by an electric drier (blower) which is placed near the lens. The specimen was placed on a specimen holder stage which was placed on a computer controlled X-Y translation stage (SVP lasers, India). A short computer program was written to control the movement of this X-Y translation stage. A thin jet of tap water was used as a containment layer. The thickness of the containment layer was maintained to be 1-2 mm throughout the experiment [23]. The water jet is also used to incessantly remove the ablated material from the specimen's surface in order to keep the surface clean during LSPwC process.

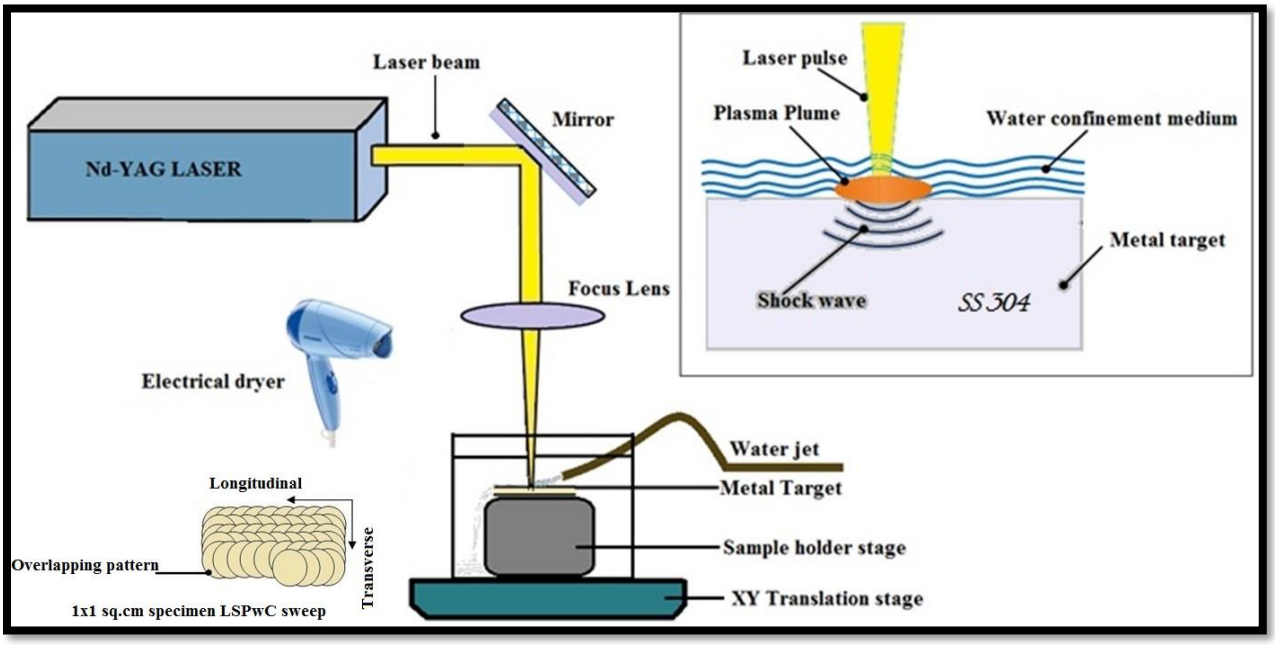

Fig.1 Schematic representation of laser shock peening without coating process setup

2.3 Characterization procedures

2.3.1 Residual stress and phase determination

The depth wise analysis of compressive residual stress estimations was taken by the X-ray diffraction $\sin^2\psi$ method [25]. The X-ray radiations of 4 mm^2 at the diffractive plane of (220) were measured by X′pert Prosystem (PANalytical, Netherlands) at a working voltage of 45 kV

and current of 40mA utilizing $Cu_{K\alpha}$-radiation with PRS X-ray detector. The residual stress calculation of the unpeened and LSPwC specimen was done by X-ray diffraction $\sin^2\psi$ method. Where "ψ" is the point between the normal to the surface and the normal to the diffraction plane. The residual stresses were measured in the σ_x direction [25]. The electrolyte polishing progressive layer removal method was chosen for profundity examination of compressive residual stress. It was carried out by applying 80% methanol and 20% perchloric acid solution by controlling voltage of 18 V with incessant electropolishing process. A high-resolution X-ray diffraction was obtained to analyze the phases of untreated and LSPwC treated specimens using X-ray instrument (Bruker D8, USA). The X-ray source used was $Cu_{K\alpha}$ radiation with a wavelength of 1.54 Å.

2.3.2 Three-dimensional surface profiling

The surface roughness of the specimen was measured utilizing surface profilometer (MarSurf, Germany). The 3-D surface topographical analysis was performed using atomic force microscope (AFM) (Nanosurf easyScan 2, Switzerland).

2.3.3 *Contact angle measurements*

The water contact angle (θ) was measured using goniometry instrument (Model Pheonix 300, SEO, Korea) at room temperature (25℃). The droplet volume of 10 μL distilled water was used to examine the surface wettability characteristics.

2.3.4 Micro/nanostructure analysis

An optical microscope (Carl Zeiss) was utilized to in investigating the microstructure of samples by using standard etchant Glyceregia (10 ml HCl, 2-3 drops of glycerine, 15 ml HNO_3 and 10 ml acetic acid) for approximately 90 seconds. For the optical microscopic studies,

$10 \times 10 \times 5$ mm unpeened and LSPwC cross-sectional specimens were utilized to analyze depth changes in the microstructure. A high-resolution transmission electron microscope (HR-TEM, FEI, Tecnai-G^2 20, Netherlands) working at 200 kV is utilized to study the microstructural characterizations. A precisely sliced and ion polished top layer of LSPwC thin foil of less than 100 μm thickness was prepared without any damage to the original specimen.

2.3.5 Mechanical studies

As per ASTM: E384 standard, the transverse cross-sectional specimen is utilized to quantify Vickers microhardness estimations with a consistent load of 1.96 N (200g) for 10 seconds [23].

2.3.6 Electrochemical examinations

A potentiostat (Sinsil Instruments, USA) was utilized to study the electrochemical corrosion behavior of the unpeened and LSPwC specimen. The potentiostat consists of three-electrode cell system with a platinum foil serves as an auxiliary electrode, a standard calomel electrode (SCE, 0.244 V vs. SHE) as a reference electrode and the unpeened and LSPwC specimen acts as a working electrode. The exposure area of 1×1 cm^2 of untreated and LSPwC treated regions were immersed in 3.5% NaCl solution at the open circuit potential for 1 h and the potentiodynamic polarization plot was determined in the range of -750 mV to 1500 mV. The studies were performed five times in order to understand the electrochemical behavior of the specimens [24]. The corrosion current density Icorr was measured using Stern-Geary equation,

$$I_{corr} = \frac{\beta_a \beta_c}{2.303(\beta_a + \beta_c) R_p} \quad \ldots (2)$$

Where βa & βc are the Tafel constant and R_p is the rest potential. Faraday's law determined the corrosion rate (CR) of the LSPwC and unpeened sample,

$$CR = \frac{I_{corr} \times K1 \times EW}{\rho} \quad \ldots (3)$$

where CR is given in mm/yr, Icorr in mA/cm2. K1 is the corrosion conversion constant which is equal to 3.27×10^{-3}, EW and ρ are the equivalent mass and density of the sample respectively.

3. Results and discussion

3.1 Residual stress distribution analysis and low energy laser pulse overlapping optimization

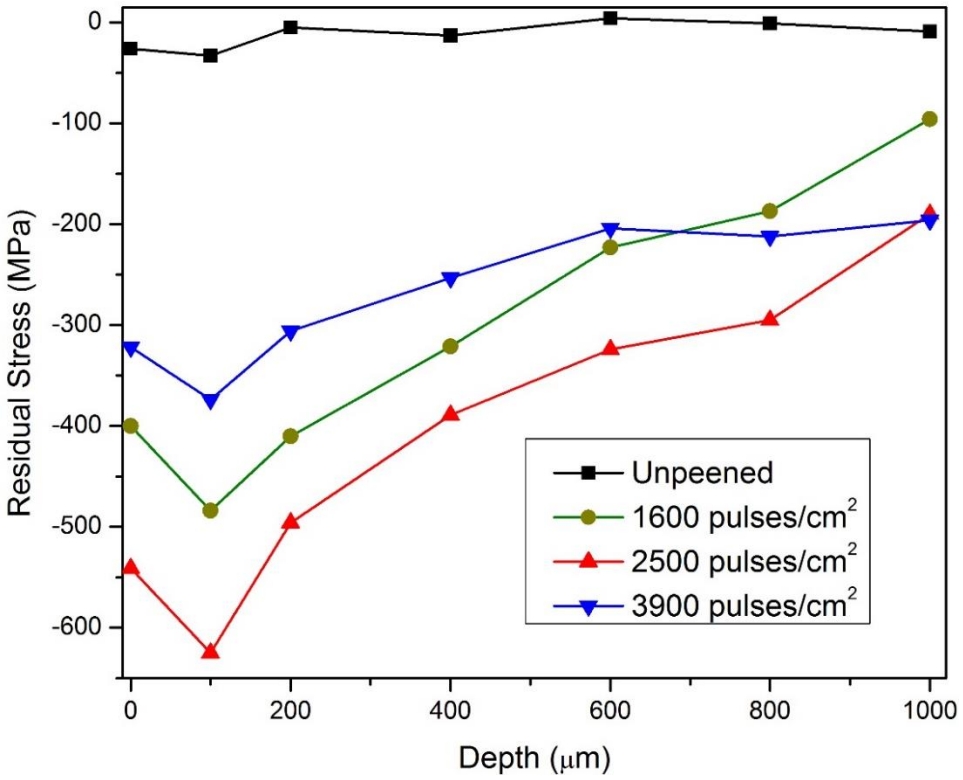

Fig.2 Compressive residual stresses induced at varying depths using different pulse overlapping via LSPwC process (Avg. standard deviation = ± 11.9 MPa)

The residual stress profiles as a function of depth at different pulse overlapping (here represented in terms of pulse density) are depicted in the **Fig.2.** In the unpeened specimen, the magnitude of the residual stress is almost zero. This leads to the fact that the initial stress has nearly no effect on the shock wave and hence can be neglected [10]. The inhomogeneity at the beginning of the graph is due to softening of the material at the surface due to the thermal effect caused by laser material interaction and also due to the surface roughness. The value of compressive residual stress goes on decreasing slowly as we go further away from the surface layer. This phenomenon occurs because the intensity of the shock waves is the maximum at near surface layer and it dwindles as it propagates further into the material.

When we contrast the residual stress profiles of different pulse densities, it is observed that maximum value of residual stress can be seen at the pulse density of 2500 pulses/cm^2 which is approximately 650 microns. For all three pulse densities, the maximum residual stress was achieved between the depths of 75-150 microns. Whereas, for the pulse density of 3900 pulses/cm^2, there was a decline in the residual stress values and which is because the thermal effect does not occur until the pulse density has reached 2500 pulses/cm^2. After the pulse density of 2500 pulses/cm^2, the thermal effect commences, and thermal relaxation of the stresses occurs. Hence at 3900 pulses/cm^2, there is a thermal relaxation of residual stresses, and the value of compressive residual stress in the specimen has decreased.

3.2.1 2-D surface roughness analysis

Table-3 Surface roughness profile for unpeened and LSPwC specimens (R_a: Average roughness; R_y: Maximum height of the profile; R_q: Root mean square roughness)

Pulse density	Pulse overlapping (~%)	R_a (µm)	R_z (µm)	R_q (µm)
Unpeened	--	0.0519	0.4197	0.0850
1600 pulses/cm^2	65	0.3577	2.3557	0.4831
2500 pulses/cm^2	75	0.3812	2.5363	0.4999
3900 pulses/cm^2	85	0.4199	2.5546	0.5276

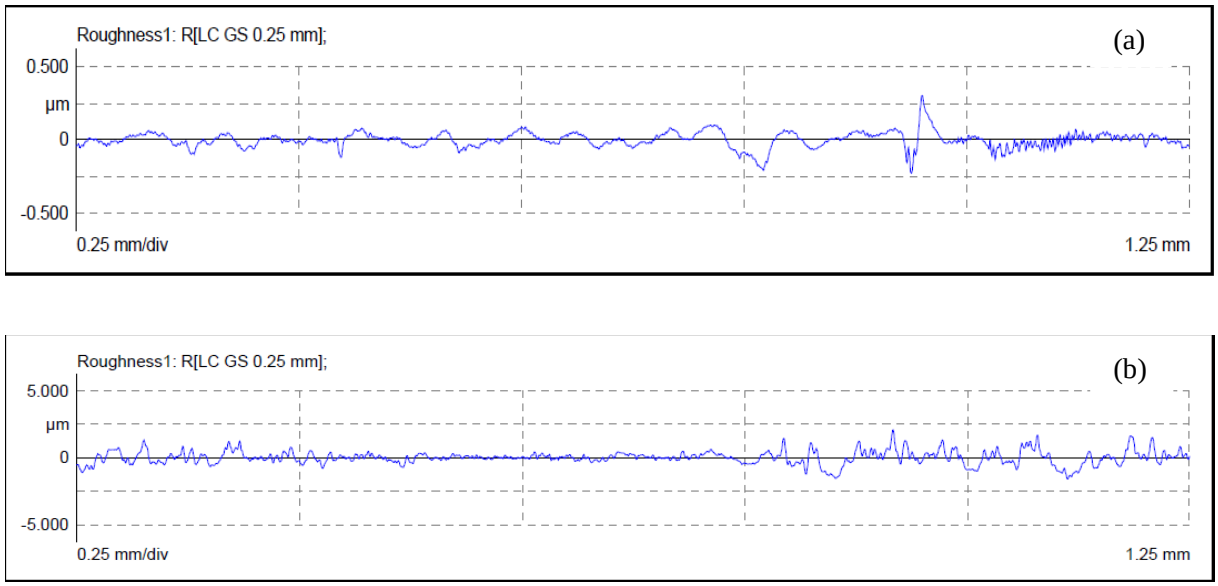

Fig.3 Surface roughness of (a) Unpeened and (b) LSPwC with 2500 pulses/cm^2 specimens using profilometer

The surface roughness values of the unpeened and LSPwC specimens are given in Table-5 taking into consideration the following factors: 1.) R_a: Average Roughness; 2.) R_z: Maximum Height of the Profile; 3.) R_q: Root Mean Square Roughness. Table-3 depicts the surface roughness values for varying pulse densities. **Fig.3a** portrays a 2-D graph showing the surface roughness of the unpeened AISI 304 austenitic stainless steel specimen, whereas, **Fig.3b** portrays

a 2-D graph showing surface roughness of the LSPwC AISI 304 austenitic stainless steel specimen with pulse density of 2500 pulses/cm^2. On contrasting **Fig.3a** with **Fig.3b,** it can be said that the surface roughness profile has been increased considerably which can be reflected from the values presented in the Table-3.

It is evidently seen from the table-3 that the surface roughness values are increasing linearly with increase in the pulse density. This is due to surface ablation of the metal surface that takes place during the LSPwC process. Higher the laser pulse density, greater the surface ablation and hence higher the surface roughness [7,16,19,23]. There is a 59%, 46% and 49% increase in the values of surface roughness (R_a, R_z and R_q respectively) of specimen 2 (2500 pulses/cm^2) when contrasted with the unpeened specimen. The pulse density of 2500 pulses/cm^2 has been considered because the maximum residual stress was obtained when the pulse density parameter of the laser was tuned accordingly. Henceforth, for all purposes, this pulse density shall be considered. Since corrosion resistance of the material depends on the surface roughness value, with a nominal and controlled increase in the roughness value the corrosion behavior was found to have enhanced, and detailed analysis is given in further section 3.7.

3.2.2 Atomic force microscopy (AFM) 3-D topography analysis

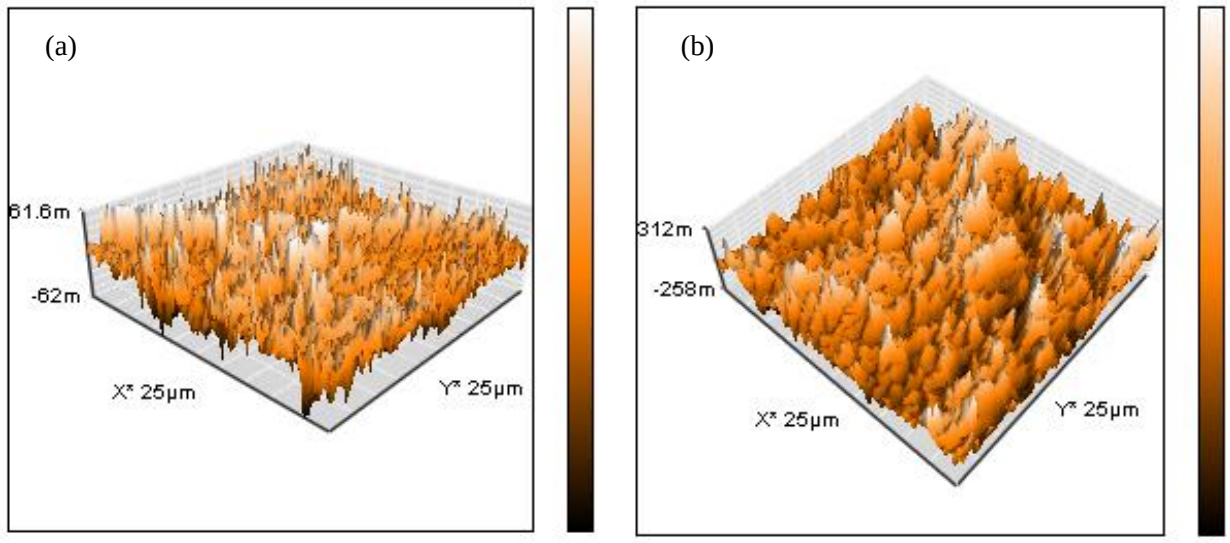

Fig.4 AFM surface 3-D topography of (a) Unpeened and (b) LSPwC with pulse density of 2500 pulses/cm^2

The **Fig.3** illustrates only the surface profile height in two dimensions; However, to better understand the topography of the LSPwC modified surface a three-dimensional topographical analysis is essential. This topographical study of the sample was done using AFM, and the results are shown in **Fig.4.** The test was performed in a range of 2 µm × 2 µm and sampling length were set as 0.5 mm. Owning to deterioration of the surface quality, the majority of the element breakdown starts at the surface [14,25]. The surface topography of the unpeened and LSPwC sample surfaces are shown in figure **Fig.4a & 4b** respectively. From the **Fig.4a & b,** it can be seen that after LSPwC process, more valleys are observed. The direct laser shot ablation is the principle reason behind the suppression of crest to the valley. Therefore from AFM surface topography [14,23], it can be seen that the LSPwC sample surface showed more surface roughness than the unpeened surface. The LSPwC process makes a nominal addition in the surface roughness of the material, and this nominal addition does not affect the corrosion resistance of the specimen. From **Fig.4b,** one can scrutinize that the surface roughening has been

achieved in a controlled yet quite an inhomogeneous manner. If the surface roughness increases beyond the limit, then it can be said that the corrosion resistance will fall and corrosion rate will increase [13,14,18]. This phenomenon occurs because increasing the surface roughness beyond the limit will open the pit sites and hence will facilitate pitting corrosion [20,29].

3.3 Water contact angle studies

When the contact angle provided by the surface roughness is >110°, it results in hydrophobicity or low wettability, whereas, if the surface has contact angle < 65° and high surface energy then it leads to hydrophilicity or high wettability [27-30]. It is clear from the roughness results (Section 3.2) that the surface roughness of the specimen has increased after the LSPwC process was performed. The surface morphology may either improve or diminish wetting, contingent upon the contours and size of the protrusions. There are two conceivable instances of solid surface wetting that may happen, which were described out quite a while prior by Wenzel and Cassie–Baxter [31]. If the liquid occupies the space in the valleys of the coarse surface then the contact angle theta is described by Wenzel's equation (**Fig.5a**); whereas on account of tapered valleys between surface protrusions it might happen that fluid sticking is repressed with the fluid staying on top of the projections. Therefore, the air is caught underneath the fluid and the fluid then sits on the surface as shown in the **Fig.5b**. In such a case the fluid contact with the strong surface is incredibly lessened and the framework is depicted by the Cassie–Baxter condition [31].

$$\cos\theta_{C-B} = \varphi_s \cos\theta - (1-\varphi_s) \quad \ldots (4)$$

Where φ_s is the portion of the fluid base in contact with the strong surface, $\varphi_s < 1$, and $(1 - \varphi_s)$ is the part of the fluid base in contact with air pockets. Air is not wetted by water and in this way

the water/air contact point equivalents to 180°. Therefore, this cosine term prompts to the negative sign in the second term of equation (4). Cassie–Baxter condition proposes that expanding the surface roughness results in superhydrophobic states [31 - 33].

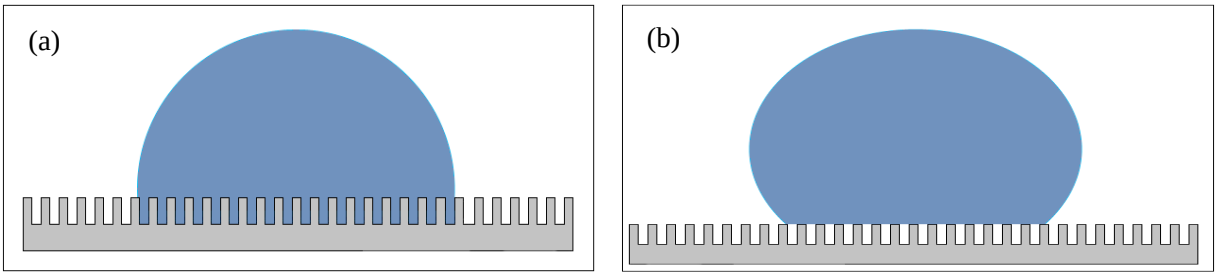

Fig.5 Wenzel and Cassie-Baxter model of wetting (a) Wenzel model (b) Cassie-Baxter model [31]

Razi *et al*. [32] irradiated steel and titanium specimens with Nd: YAG laser with a wavelength of 1064 nm and concluded that the contact angle decreases with increasing the laser fluence. They also found that that the effect of laser pulse number is not as important as laser fluence in some cases. In this study however it is found that the contact angle increases after the single impact LSPwC process. The contact angle of the unpeened specimen was measured to be 34.24˚(**Fig. 6**) i.e the surface was hydrophilic in nature.

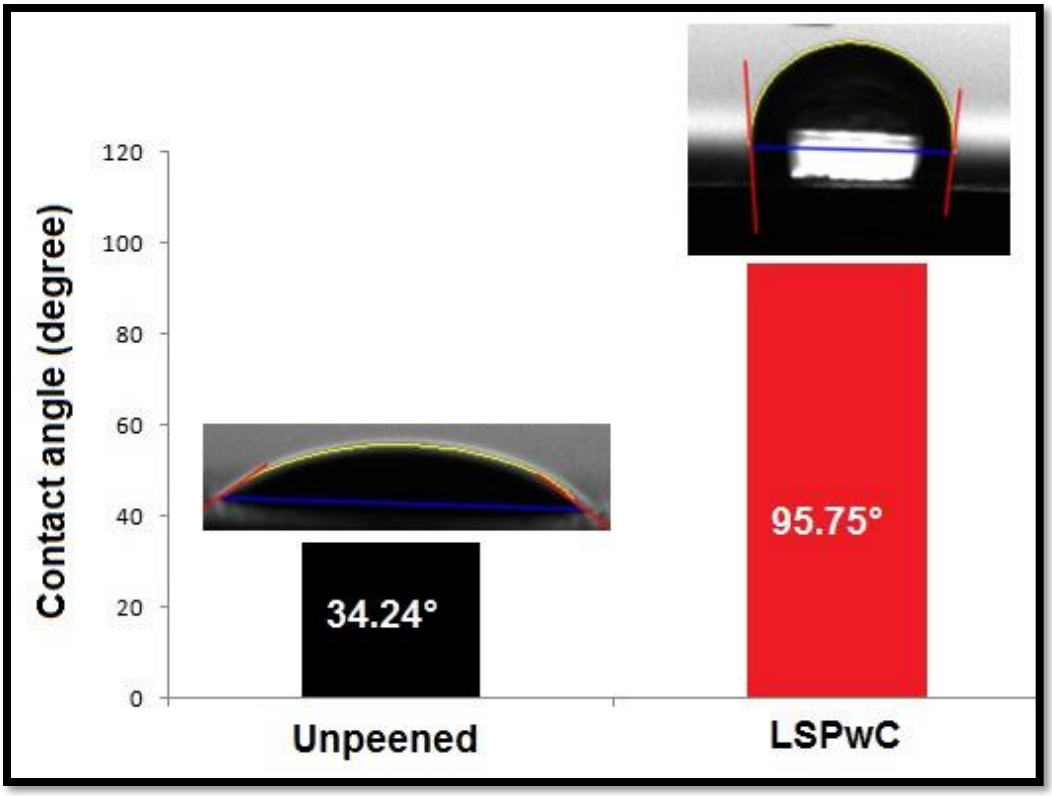

Fig.6 Contact angle of the unpeened and laser shock peening without coating specimens

However, after the LSPwC single impact process, the contact angle was increased and was measured to be 95.75˚(**Fig.6**) which implied that the surface turned to hydrophobic nature. This is due to the alteration in the surface free-energy and changed surface morphology. It was previously [32] found that when the surface roughness is increased the contact angle is reduced. Owning to this, it can be said that the contact angle of LSPwC specimen is lower than that of untreated specimens in most of the cases. However, contact angle is a function of surface roughness as well as surface-free-energy. The high uneven surface roughness or the oxide layer might be the cause for increased contact angle. This oxide layer is formed on the surface amid the LSPwC process due to laser and material interaction in presence of water. When the oxide layer is formed, the surface-free energy was altered. Since the surface-free energy played an important role in the surface reactions, it is a determining factor for contact angle. Another

advantage of peening is that it removes the surface contamination such as dirt which has low surface energy. Thus, all these factors lead to an elevated contact angle making it hydrophobic [34]. The fact that the contact angle has increased after LSPwC process and the surface is turned to be hydrophobic nature is an advantage for the material as hydrophobicity of the materials surface helps in resisting against corrosion. This is because the water molecule will be repelled by the metal surface and thus further the oxidation reaction will be averted.

3.4 High-resolution X-ray diffraction phase analysis

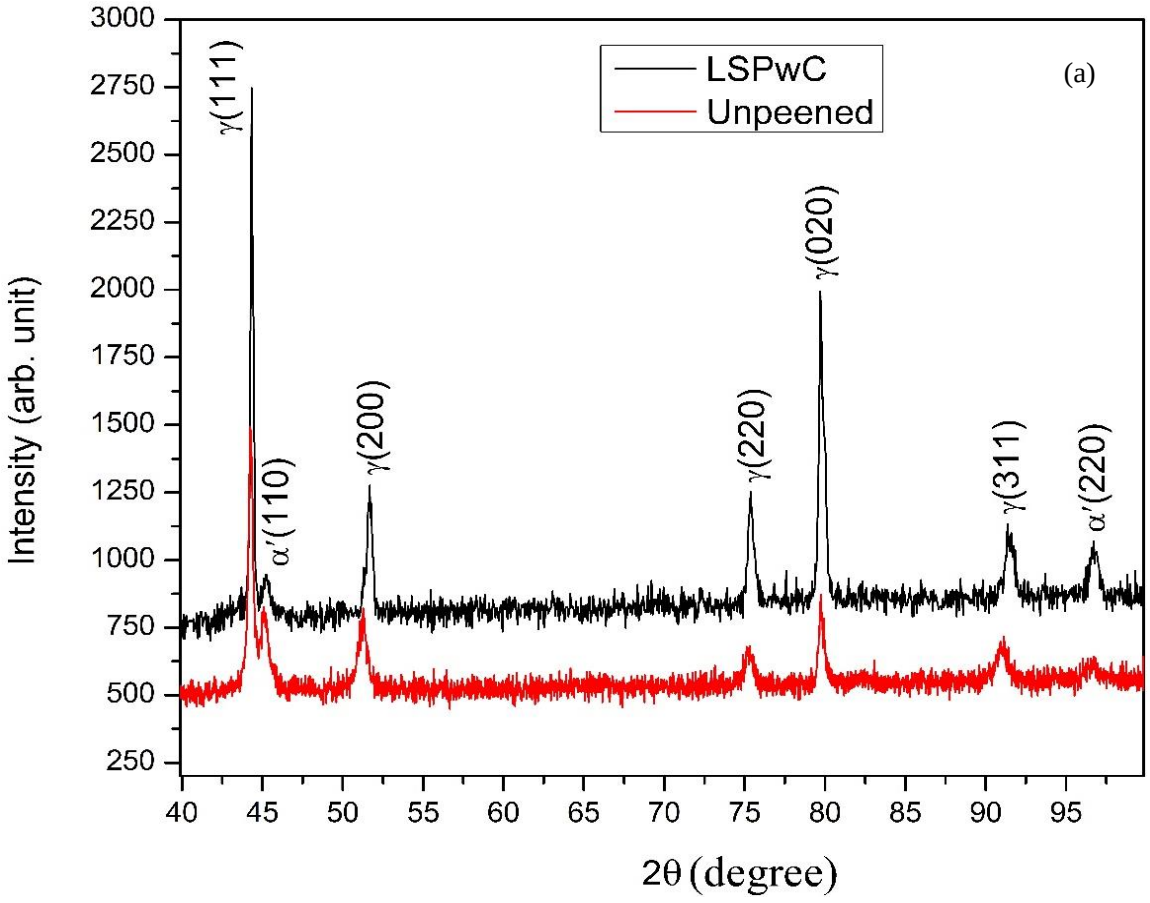

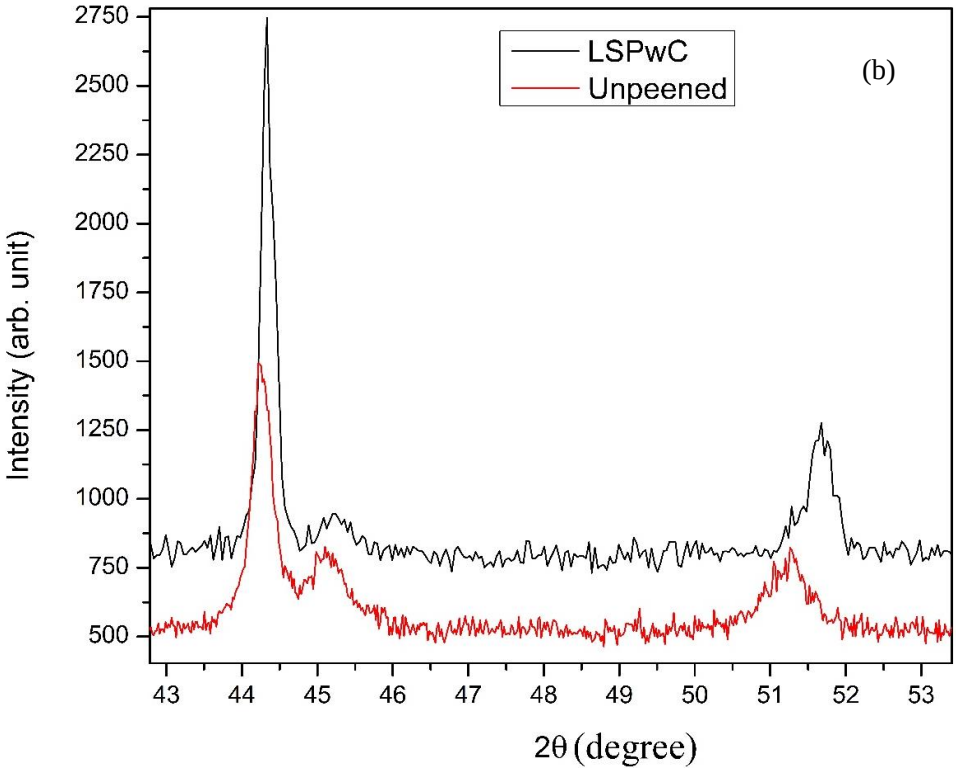
LSPwC
Unpeened
(b)
Intensity (arb. unit)
2θ (degree)
2750
2500
2250
2000
1750
1500
1250
1000
750
500
43
44
45
46
47
48
49
50
51
52
53

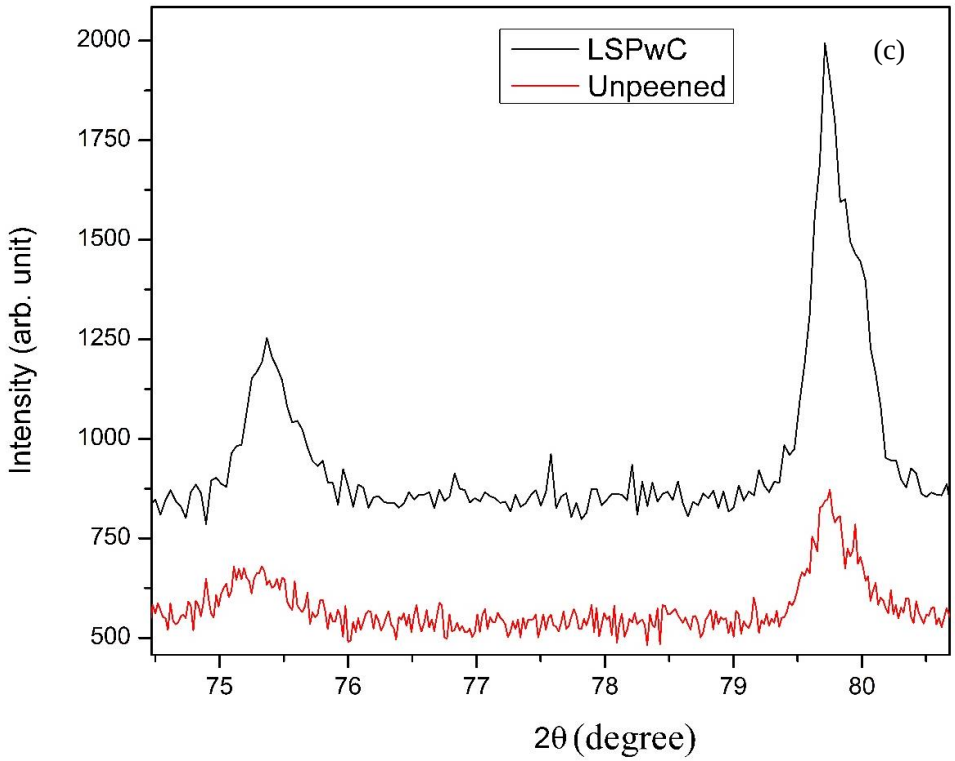
LSPwC
Unpeened
(c)
Intensity (arb. unit)
2θ (degree)
2000
1750
1500
1250
1000
750
500
75
76
77
78
79
80

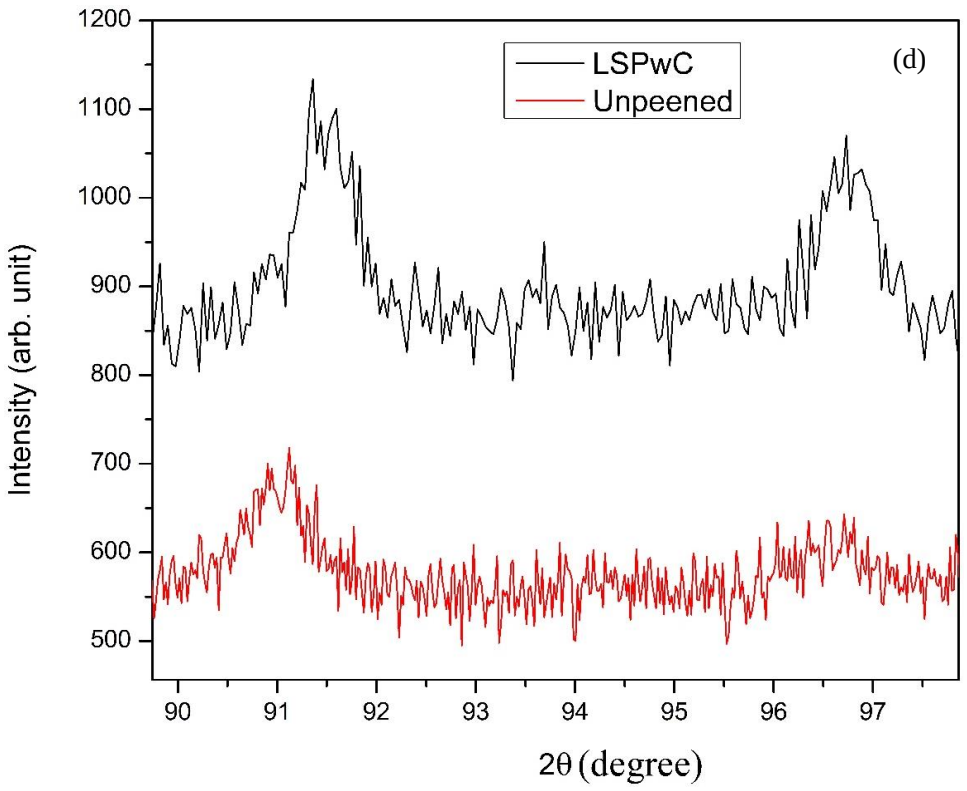

Fig.7 High-resolution X-ray diffraction pattern of AISI 304 austenitic stainless steel before and after laser shock peening without coating process (a) Indexed XRD graph (b, c and d) Magnified images of XRD

Fig.7 depicts the X-ray diffraction profiles of the unpeened (black) and LSPwC (red) specimen. In the preceding studies [10, 5], strain instigated martensite transformation trend was seen after the LSPwC on 304 austenitic stainless steel as a result of near-surface plastic deformations. This was due to conventional surface treatment systems like deep rolling, shot peening, and surface mechanical attrition treatment (SMAT) [10, 11]. On scrutinizing **Fig.7a,** it can be said that peaks of γ and α′ are present in both unpeened and LSPwC specimens. It can be said that solution annealing and water quenching did not create perfect austenitic microstructure. This can be evidently seen from (**Fig.7a**) the α′(110), and α′(220) peaks present in the unpeened specimen [35]. A.K. De *et al*. [36] in their research has found evidence of formation of

hexagonal ε-martensite phase amid the deformation. However, no such evidence of hexagonal ε-martensite was discovered in the present study. The body-centered cubic (BCC) structure of martensite also known as α-martensite was found at the peak of α′ (110). The peaks γ (220) and γ (311) are the reflections of austenite phase [36]. It is evident from **Fig. 7(b, c & d)** that there is a noticeable peak shift towards the higher 2θ angles after the LSPwC process was complete-implying that there is lattice strain induced in the crystal lattice.

Peaks can be seen at around the angles of 43, 45, 52, 75, 80, 91 and 96˚ in the **Fig.7(a)**. Also there is a noticeable shift in the γ-phase at the angle of around 43˚ towards α'-phase present at angle of around 45˚. This indicated that there is a beginning of martensitic transformation in the material. From **Fig.7a & 7d**, it can be seen that the α′ (220) peak which was not so prominent in the unpeened specimen had an elevated intensity in the LSPwC treated specimen. This difference in the relative intensities of the two peaks was indicative that the martensite phase was forming as a result of deformation induced by the LSPwC process. The peak shift towards the higher 2θ angle can be seen evidently in **Fig.7d.** This implied that the lattice parameter was decreasing, thus, supporting the previous statement. These results are consistent with the prior results surveyed in the literature [35-39]. The developments of martensitic phases which are induced as a result of the manufacturing process are a typical feature for austenitic stainless steels, which relies on temperature, strain and the strain rate [40]. However, Mordyuk *et al*. [40] did not discover the existence of deformation incited martensite in the LSPwC specimen without coating. The elevated intensity of the (111) peak after LSPwC process is an indicating factor of the induced residual stress in the sample. This phenomenon may be explained with the help of Bragg's law of diffraction. The internal residual stress directly affects the crystal lattice structure and, hence, affecting the lattice spacing.

3.5 Microstructure analysis

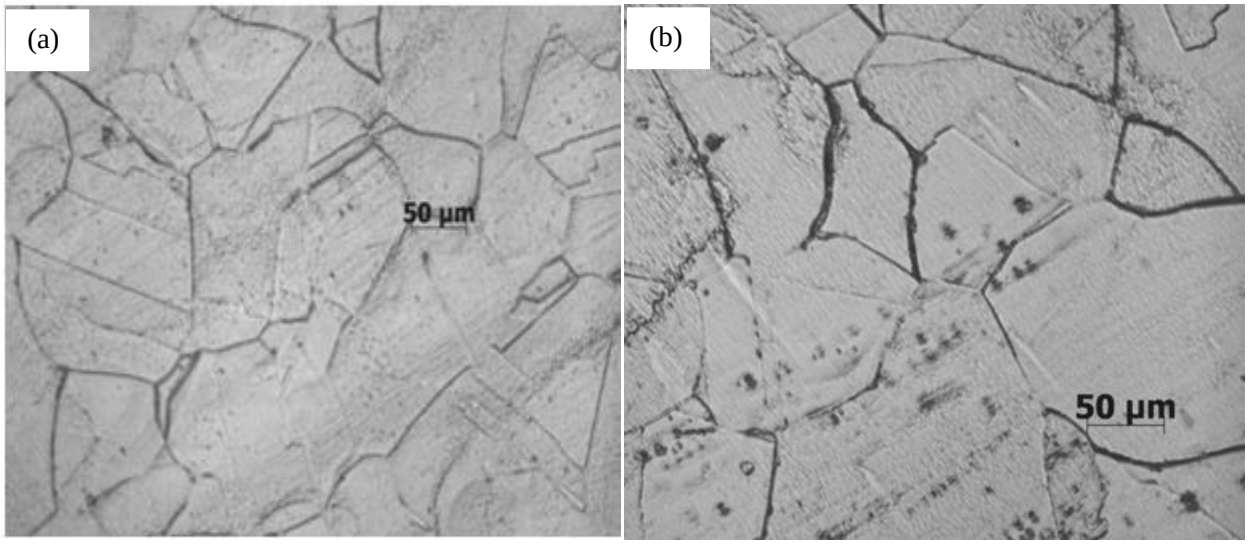

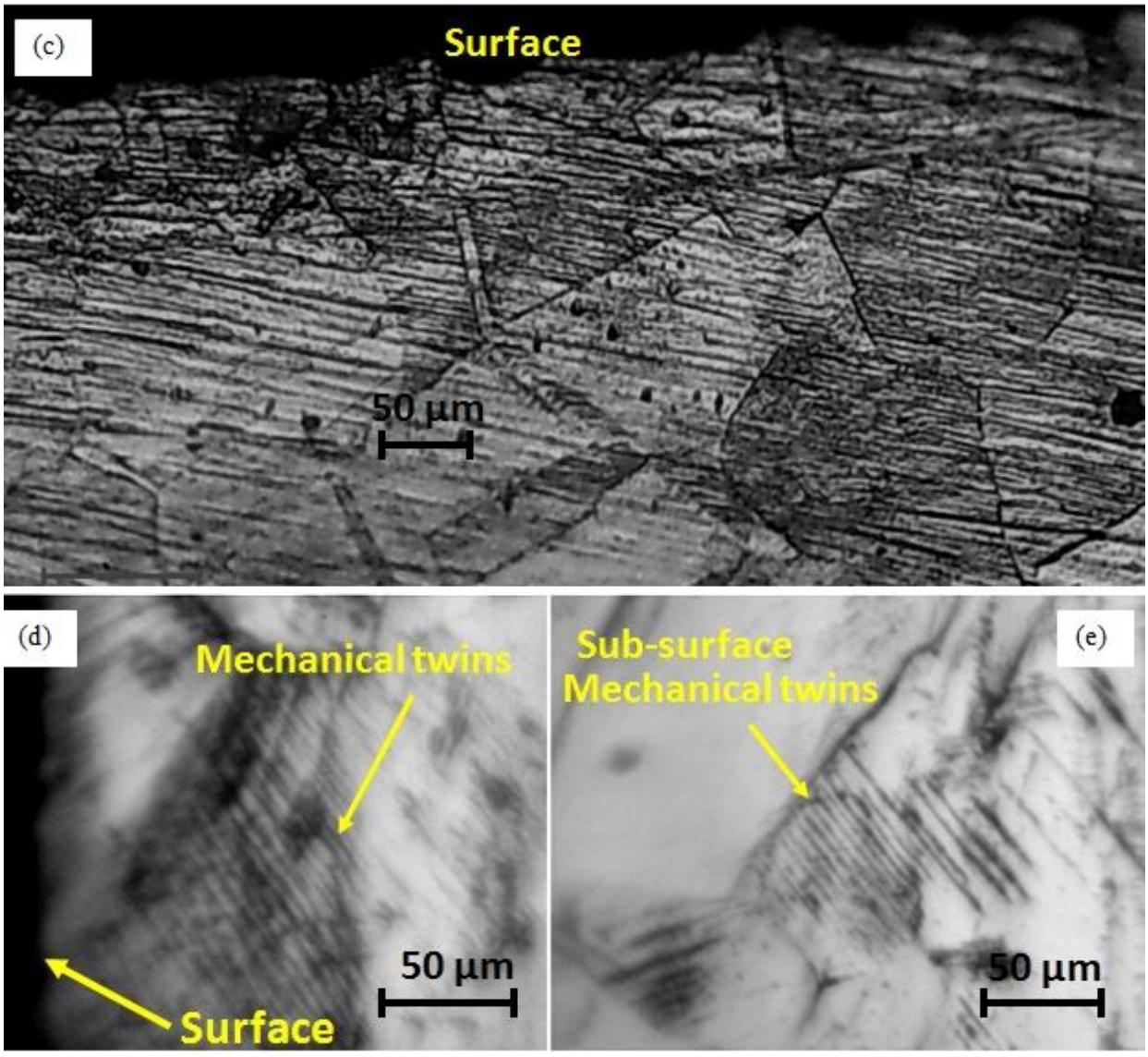

Fig. 8 The cross-sectional optical microstructure of AISI 304 austenitic stainless steel (a, b) Unpeened [16] and (c) LSPwC near surface (d) LSPwC sub-surface region

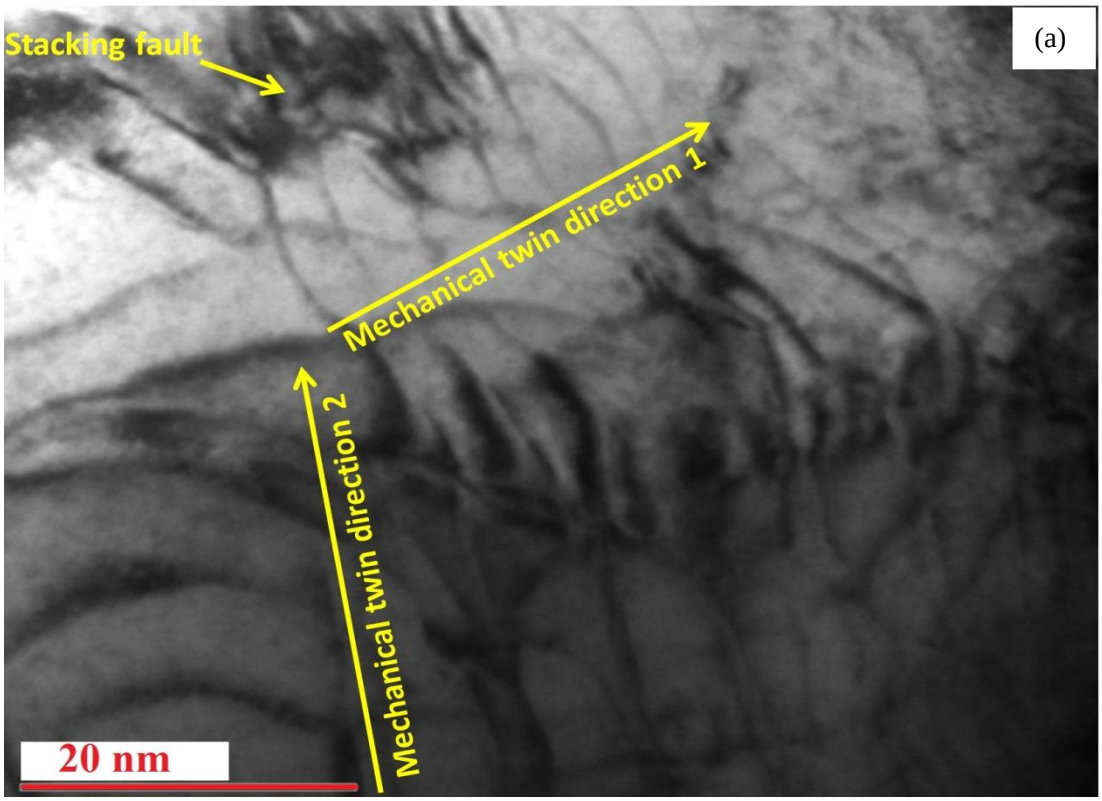
(a)
Stacking fault
Mechanical twin direction 1
Mechanical twin direction 2
20 nm

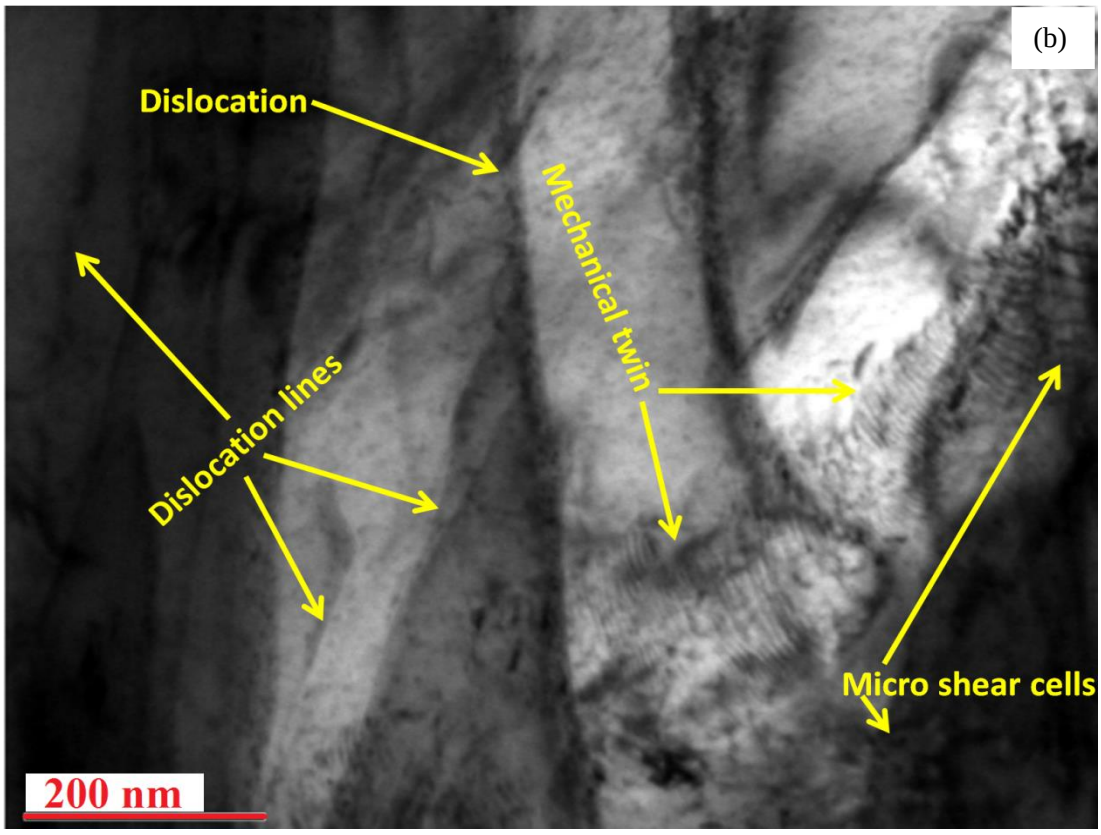
(b)
Dislocation
Mechanical twin
Dislocation lines
Micro shear cells
200 nm

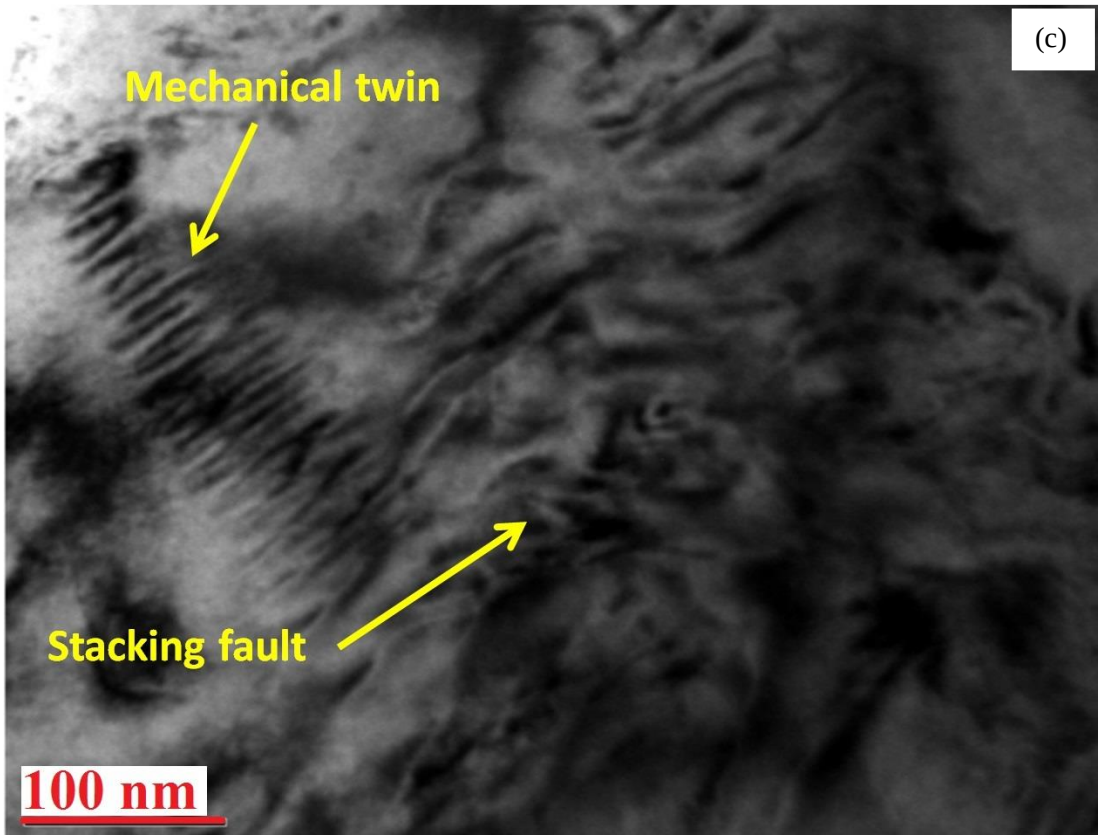
(c)
Mechanical twin
Stacking fault
100 nm

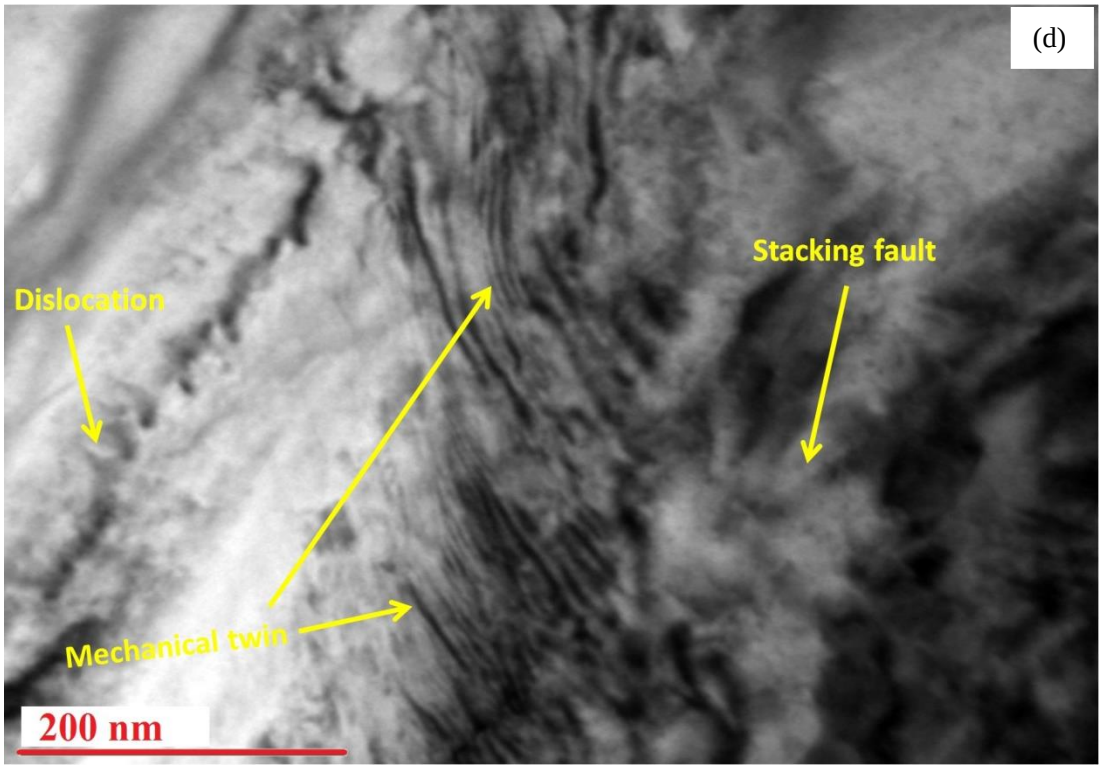
(d)
Stacking fault
Dislocation
Mechanical twin
200 nm

Fig.9 High-resolution transmission electron microscopic images of top layer (50 microns) of LSPwC specimen (a) Multidirectional twins and (b, c & d) deformation induced microstructural refinement features such as dislocations, mechanical twins, micro shear cells and stacking faults

The optical microstructure of AISI 304 austenitic stainless steel has been shown in **Fig. 8a & b**. **Fig.8c & d** showed deformation-induced microstructural refinement features is identified as mechanical twinning (MT) [9,11,41]. Also of **Fig.9,** the high-resolution transmission electron microscopic (HR-TEM) investigation on the major plastic deformation layer (top 50 microns surface of LSPwC region) revealed few other microstructural grain refinement features such as multidirectional mechanical twins, stacking faults, micro-shear cells, dislocations and dislocation slip lines. It can be observed that the two different directions of mechanical twins and its intersections in **Fig.9 (a)** and from these experimental observations, it can be said that the severe plastic deformations were taking place on the surface of the specimen.

Also, the fact that low energy laser shock processing induced the severe or major plastic deformation depth was less compared to Lu et.al's [9,11] studies using the high energy multiple laser shock processing. Also, it is anticipated that the increasing strain will induce more multidirectional mechanical twins. Further, the multiple laser shock peening will be investigated in the near future. Also, it is well proved that the nanosecond high power and low energy laser pulses are inducing high strain in specimens, and it plays a significant role in observing those surface grain refinement features. The austenitic stainless steel has low stacking fault energy (SFE) (18 mJ/m^2) and therefore, maximum numbers of twins are observed. Metals with low SFE adopt a twinning mechanism to account for the deformations introduced in the crystal lattice [38]. Mechanical twinning occurs in face-centered cubic (FCC), body-centered cubic (BCC) and

hexagonal close-packed (HCP) structures when it is highly strained; as they don't have sufficient slip systems to account for the arbitrary shape changes.

Dislocation slip and deformation twinning are two processes which occur simultaneously when we plastically deform austenitic stainless steel. The threshold stress should be attained in order for deformation twinning to initiate. Chen *et al*. [41] revealed a way to describe this threshold stress as

$$\sigma_T = 6.13 \frac{\gamma_{SFE}}{b_p} \quad \ldots (5)$$

Where 'γ_{SFE}' represents stacking fault energy while 'b_p' stands for Burgers vector of Shockley partial dislocation. On substituting the values, we calculate the threshold stress for AISI 304 austenitic stainless steel to be around 584 MPa [42, 43]. So it can be safely assumed that the stress produced in the near surface and a subsurface layer of the material is greater than 584 MPa and mechanical twins are observed. From the residual stress distribution (**Fig.2**) one can observe that the maximum amount of residual stress is obtained near the surface region. Since we are dealing with compressive residual stress, the threshold stress should be -584 MPa. On scrutinizing **Fig.2,** it can be said that considering the threshold stress limit for twinning in AISI 304 austenitic stainless steel, the deformation twinning must occur in depth between approximately 50 and 140 µm. From **Fig.8c & 8d** it can be said that twins were observed at the same depth as predicted in the ongoing discussion. However, the twin density was observed to vary as a function of depth. It was found to be maximum at 50 µm and went on decreasing with further depth. This is because of the fact that the stress levels are at the peak point near the surface and keep decreasing with depth. Deformation twins are easier to form on (111) slip planes [44], and hence more deformation mechanical twins can be observed. The multi-

directional alignments of microstructural twins play a significant role in the grain refinement of a plastically deformed layer of FCC metals along the depth direction with low stacking fault energy.

By reviewing the literature [42-45], it can be said that in austenitic steels a major way to deal with severe plastic deformation (SPD) is through martensitic phase transformation. Plastic deformation is responsible for producing defects in the material like dislocations, stacking faults and deformation twins [42]. From the HR-XRD results (Section 3.4) there is a trend observed towards martensitic transformation which is supported by the formation of deformation twins the first step towards martensite transformation.

3.6 Vickers microhardness analysis

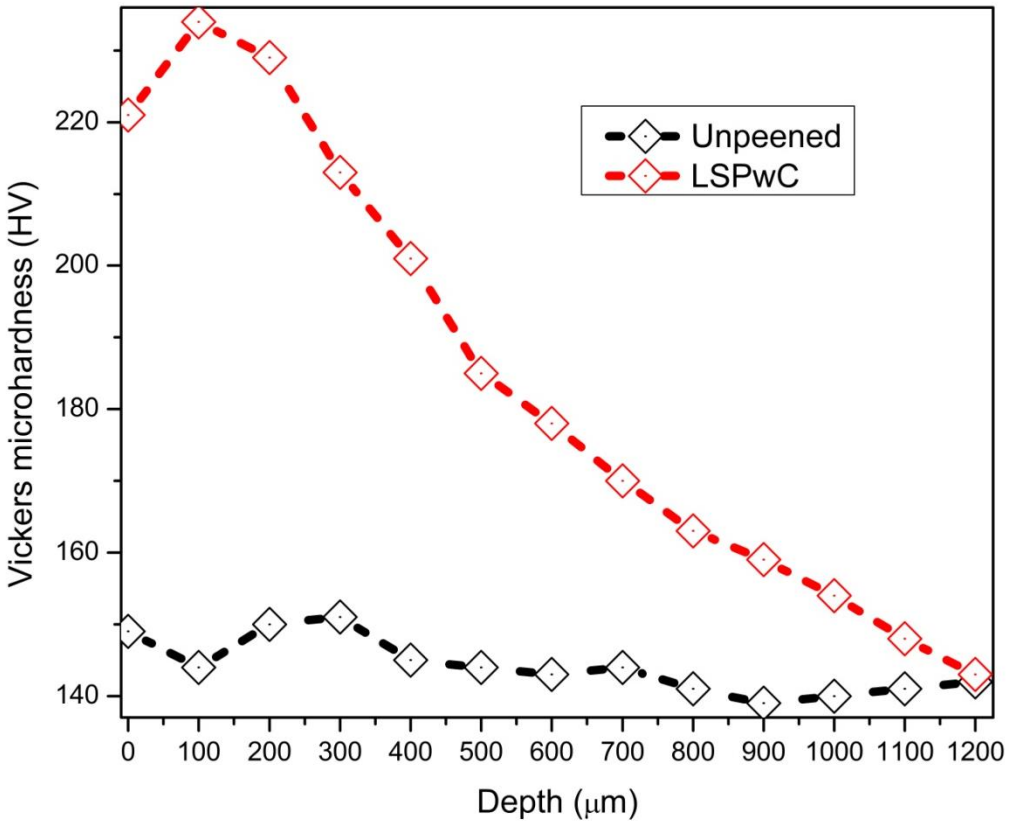

Fig.10 Depth wise Vickers microhardness variation profile for the unpeened and LSPwC specimens (Avg. standard deviation = ± 6.0 HV)

The graph in the Fig.10 depicts the Vicker's microhardness values as a function of depth for single impact LSPwC specimens. This is considered for the optimized pulse density, i.e., for 2500 pulses/cm^2. The average Vicker's microhardness of the as received specimen was 144.07 HV. The average Vicker's microhardness of the LSPwC treated specimen was 184.46 HV. The average hardness value of LSPwC specimen was increased by 28% than the as received unpeened specimen. The Vickers hardness number was defined as the load divided by the surface area of indentation. When the specimen was LSP treated, there is work hardening effect taking place till certain depth. This work hardening effect is essentially the strengthening of the material due to the plastic deformation produced. The strengthening occurs as a consequence of the dislocations generated and dislocation movements within the crystal structure [19, 7]. The work hardening effect can be explained as a consequence shock waves created in the LSP process. Due to the shock waves, dislocation lines are generated. These dislocation lines start moving across other dislocations. As the material undergoes further deformation, more and more dislocations start to slip in the material from different directions in different slip planes. Eventually, dislocation density increases and the free area where the dislocation lines could slip is narrowed down, thus, hardening the material [9].

At the surface, the hardness is seen, to begin with, a lower value in case of LSPwC specimen. This can be because of thermal effects at the surface and the surface roughness. LSPwC includes an elevation in thermal energy at the surface which brings about the softening of the material at the surface [16,23,25]. The hardness reaches a maximum value at the depth where CRS (Compressive Residual Stress) reaches its peak value in case of LSPwC specimen

and then goes on decreasing gradually. Such thermal effects are observed only at the surface of the material; they cannot be observed inside the material.

3.7 Electrochemical analysis

3.7.1 Potentiodynamic polarization studies

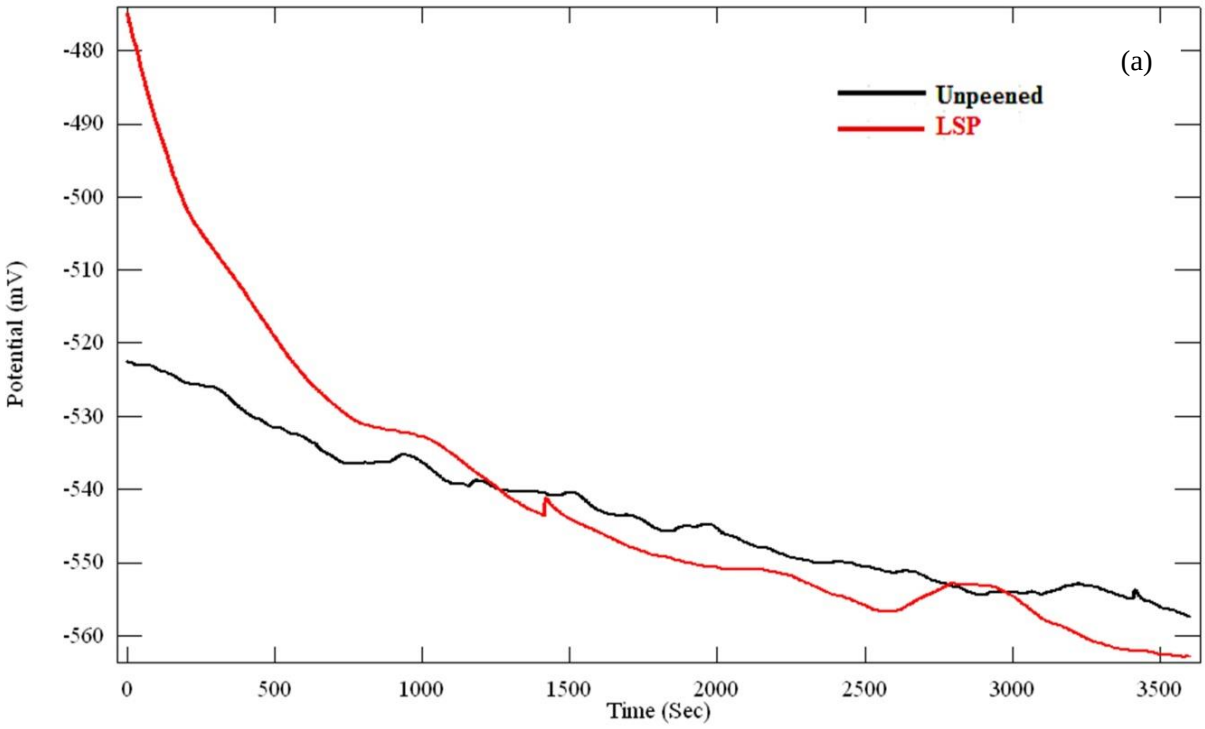

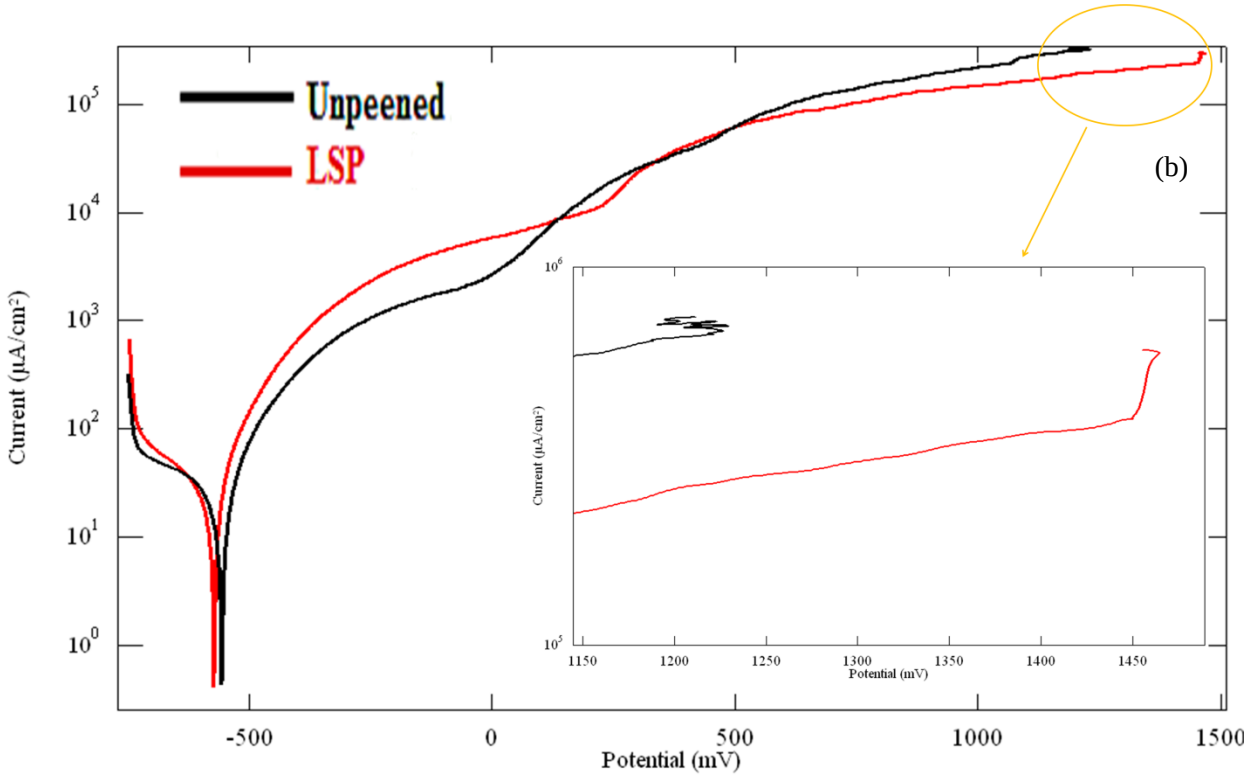

Fig. 11 Potentiodynamic polarization curves for unpeened and LSPwC AISI 304 austenitic stainless steel (a) Potential-time curve (b) Potentiodynamic polarization plot

The specific exposure area of 1×1 cm^2 unpeened and LSPwC specimens were taken for the electrochemical studies. **Fig.11 (a)** shows the open circuit potential (OCP) of the unpeened and LSPwC specimen. The OCP value of LSPwC sample at the beginning and end are -470 mV & -570 mV, whereas, the potential of the unpeened sample are -520 mV & -555 mV. As the time increases, the potential of LSPwC tends to decrease due to the LSPwC induced surface roughness. The potentiodynamic polarization plot for unpeened and LSPwC are shown in **Fig.11 (b).** The corrosion potential Ecorr and corrosion current density Icorr were determined from the plot, and the results are tabulated. From the plot, it was observed that the Ecorr and Icorr value of LSPwC sample were almost similar to the unpeened sample. Further, the corrosion rate (CR) of

the LSPwC sample (0.163 mm/yr) was also shown to be similar to the unpeened sample (0.159 mm/yr).

The laser peening on metallic materials induces various surface topographical changes such as generation of compressive residual stresses in the near surface region, grain refinement, phase transformation and an increase in surface roughness due to laser ablation. It is well known that these surface changes have a direct impact on the electrochemical activity of the metallic materials. Particularly, the surface roughness has a detrimental effect on the formation of the passive film due to the increase in exposed surface area [46-49]. However, in our case, there is no considerable change in corrosion potential (Ecorr = -570.9 mV) and corrosion current density (Icorr = 0.013 mA/cm^2) for LSPwC sample compared to the unpeened sample (Ecorr = -555.5 mV, Icorr =0.018 mA/cm^2). This suggested that the surface roughness did not have much influence on the corrosion behavior and it is consistent with the previous results [7,8,29,50-52].

Another factor which influences the corrosion behavior is the phase transformation during laser shock peening. In the section (3.4), it is observed that the LSPwC induces a phase transformation from austenite to strain induced martensite. In fact, this phase transformation leads to decrease corrosion resistance due to the galvanic coupling effect between the austenite and martensite phases [50]. However, in the present study, the corrosion rate of the LSPwC sample was similar to that of the unpeened sample, even after a phase transformation trend was observed.

In the anodic region, the LSPwC sample showed better corrosion properties. As the potential increased, the corrosion current density (Icorr) for LSPwC decreased. This meant a lesser material dissolution. Another notable observation is that the improvement in the pitting and breakdown potential. The pitting potential of LSPwC sample was 1450 mV, whereas, the

unpeened sample was only 1225 mV indicating that the repassivation ability of the LSPwC sample has been enhanced (Table-4). The reason for improvement of pitting potential can be attributed to the generation of compressive residual stress and grain refinement feature. In the present study, a grain refinement feature such as mechanical twins has been observed after the LSPwC and also it has been reported that the grain refinement in AISI 304 austenitic stainless steel can significantly improve the corrosion resistance. Further, the generation of compressive residual stress in the surface layer has a beneficial effect on the formation of the passive film, thereby, enhancing the pitting resistance of the LSPwC sample [48].

From **Fig.12(a),** it was indicative that the unpeened specimen deteriorated by severe pitting attack, thus, individual pits clubbed together and prolonged the area of aggression. Further, the pit size on the LSPwC specimen was comparatively smaller as shown in **Fig.12 (b).** This is another remarkable result achieved in the current work and indicated that the LSPwC was considerably resisting the initiation of pitting corrosion [7,8,29,47,52]. The corrosion pitting formation mechanism of unpeened and LSPwC specimens are shown in **Fig. 12(c)** & **12(d)** respectively. Another surprising result was observed in the section-3.3 is that the contact angle of LSPwC sample turned from hydrophilic to hydrophobic which causes the water molecule to slide over the metallic surface without leaving any traces of water. This hydrophobic transformation might also be responsible for the improvement in pitting resistance. The author's previous reports and most of the studies in the literature are illustrating that the corrosion pit initiation is one of the major reason for crack initiation and propagation which leads to fatigue fracture [24,36,53]. So, from the current study, it is well proved that the pitting resistance of LSPwC processed specimen could serve to extend the fatigue life of austenitic stainless steel [53].

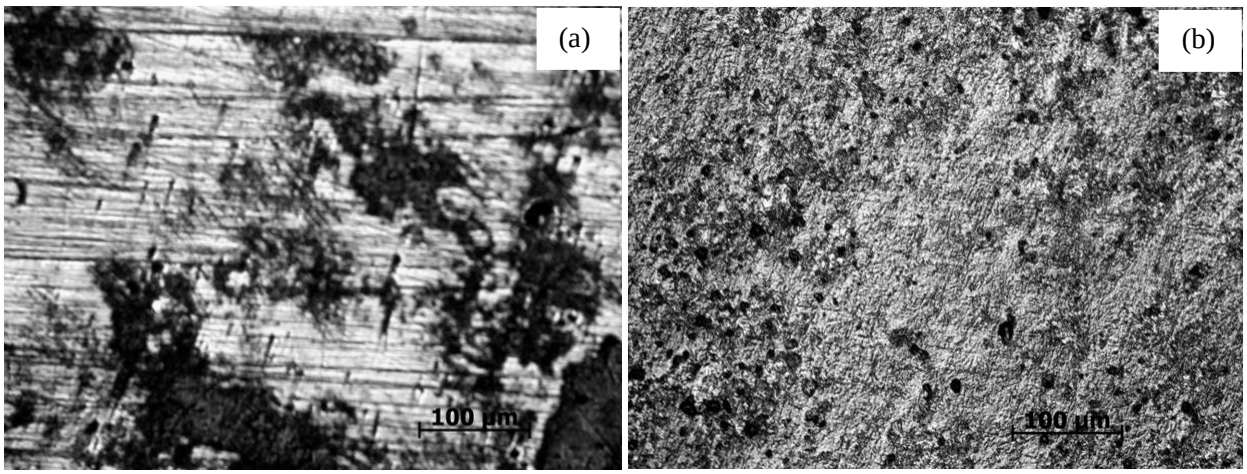

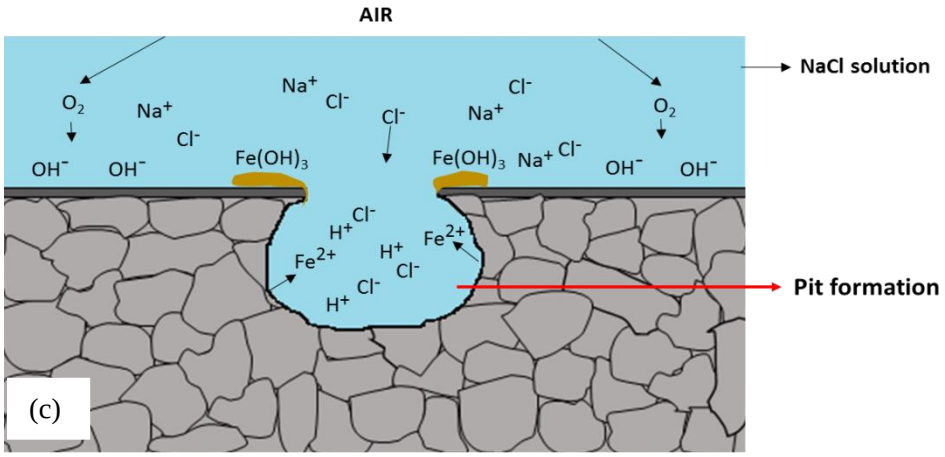

Unpeened 304 SS

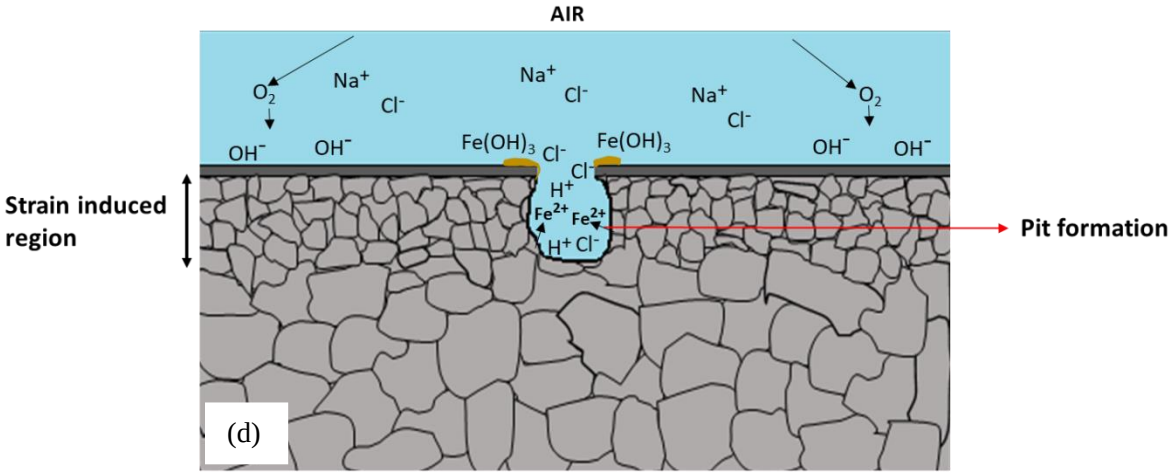

LSPwC 304 SS

Fig. 12 Corrosion pits on the surface of (a) Unpeened and (b) LSPwC treated specimens after electrochemical tests; Fig. 12 (c) & (d) shows the corrosion pit formation mechanism of unpeened and LSPwC specimens respectively

Table- 4 Electrochemical properties of AISI 304 austenitic stainless steel

Sample	E_{corr} (mV)	I_{corr} (mA/cm^2)	Corrosion rate (mm/yr)
Unpeened	-555.5	0.013	0.159
LSPwC	-570.9	0.018	0.165

3.7.2 Electrochemical impedance spectroscopic (EIS) studies

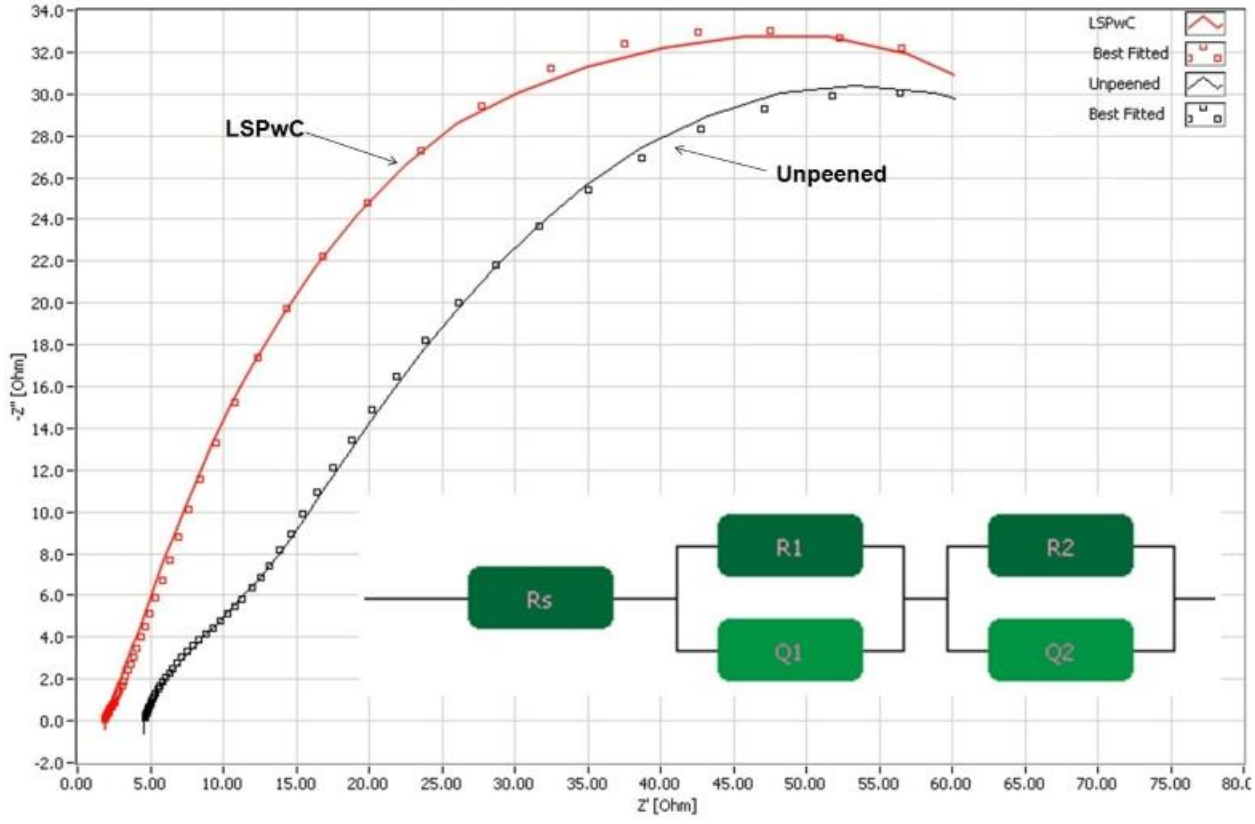

Fig. 13 Nyquist plot of unpeened and LSPwC AISI 304 austenitic stainless steel specimens tested in 3.5% NaCl solution [Inset: equivalent circuit of unpeened and LSPwC specimens]

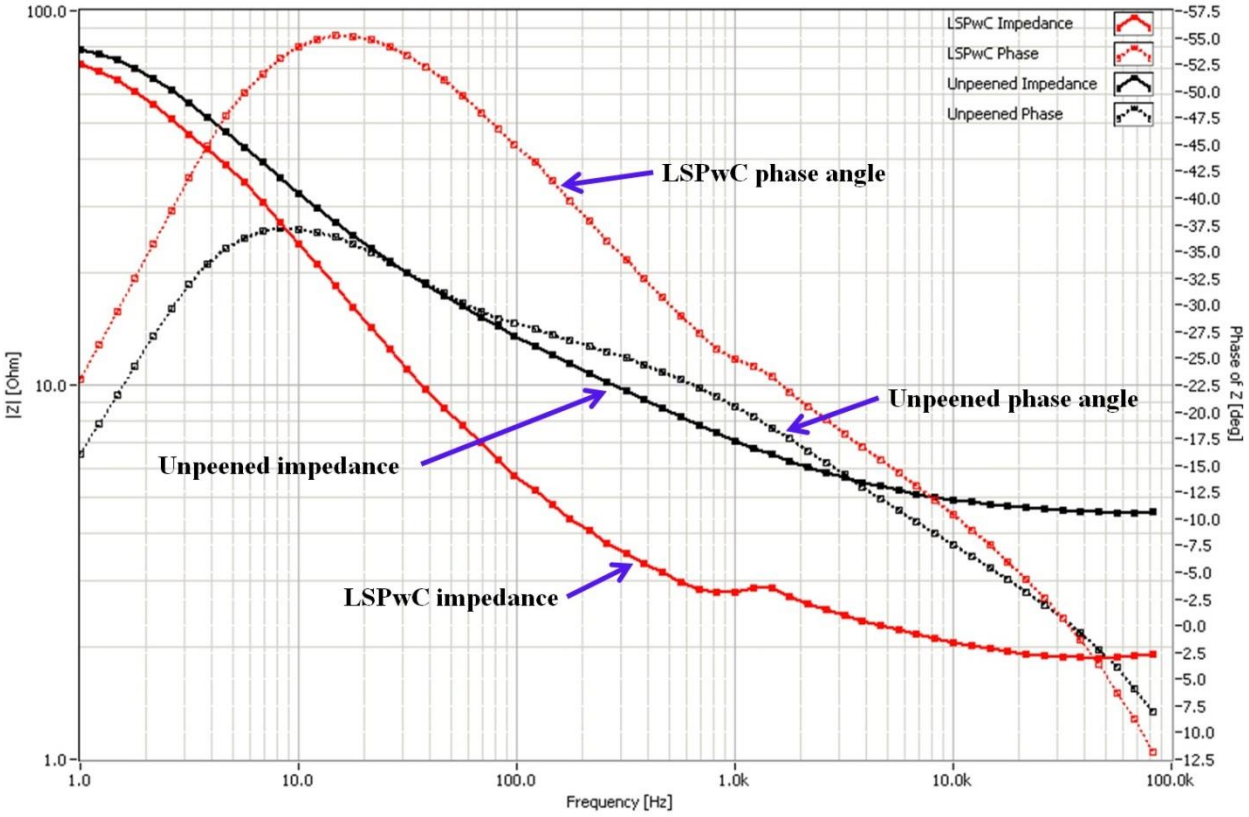

Fig. 14 Bode impedance and Bode phase angle plots of unpeened and LSPwC treated AISI 304 austenitic stainless steel

In order to compare the characteristics of passive films on unpeened and LSPwC specimens, they were subjected to electrochemical impedance spectroscopic (EIS) studies. **Fig.13&14** shows the Nyquist and Bode plot for unpeened and LSPwC specimen respectively. A simplified equivalent circuit inset **Fig.13** was used to model EIS data obtained experimentally. The equivalent circuit comprises of resistance and constant phase element (CPE), whose impedance is defined as $Z_{CPE} = [Q (j\omega n)]^{-1}$ with 'n' less than 1; for an ideal capacitance n = 1. The resistance Rs, R1 and R2, corresponds to solution resistance, the oxide layer and charge

transfer resistance respectively. The constant phase elements Q1&Q2 corresponds to the capacitance of outer layer and inner layer respectively. The EIS fitted parameters are given in the Table-5. **Fig.13** presents represent Nyquist plots for unpeened and LSPwC of AISI 304 austenitic stainless steel specimens. From the plot, it was evident that LSPwC specimen possesses better resistance properties compared to unpeened sample by exhibiting higher resistance compared to the unpeened specimen. Further, the polarization resistance Rp (Rp = R1+R2), for LSPwC specimen (193 $\Omega.cm^2$) was higher when compared to unpeened specimen (96 $\Omega.cm^2$).

The Bode impedance and Bode phase angle plots of unpeened and LSPwC are shown in **Fig.14.** The Bode phase angle maximum for LSPwC was 55°, whereas for the unpeened sample was 37°. In general, the near capacitive system exhibits phase angle maximum at 90°, and it remains constant for a wider frequency [29,46]. However, in the present study, the phase angle maximum was below 90° for both unpeened & LSPwC sample and also shows inflections on both the higher and lower frequency side. But, when compared to the unpeened specimen, LSPwC exhibits higher phase angle which evidences a stable passive film formation and hinders charge transfer process whereas the lower phase angle of unpeened specimen suggests a defective passive film formation. It is noteworthy to mention that the word done by Balusamy *et al*. [46] observed detrimental corrosion behaviour for AISI 304 austenitic stainless steel when subjected to surface mechanical attrition treatment (SMAT) due to increased surface roughness and phase transformation [29,46,52]. However, in our present study, the influence of laser peening on AISI 304 austenite stainless steel exhibited an enhanced corrosion resistance, which confirms that the surface roughness and phase transformation has no detrimental effect.

Table-5 EIS parameters of unpeened and LSPwC specimens of AISI 304 austenitic stainless steel in 3.5% NaCl solution

Specimen	R_s ($\Omega.cm^2$)	R_1 ($\Omega.cm^2$)	Q1 (Ω^{-1} cm^{-2} s^n)	n_1	R_2 ($\Omega.cm^2$)	Q2 (Ω^{-1} cm^{-2} s^n)	n_2	Phase angle (°)
Unpeened	4.528	7.5	0.78	0.93	88.3	1.56	0.74	37
LSPwC	1.76	40.6	10.02	0.94	152.2	1.26	0.77	55

4. Conclusion

(1) The compressive residual stress instigated in the material increased till it reached the pulse density of 2500 pulses/cm^2. There was a decrease in the values of residual stress for 3900 pulses/cm^2 due to thermal relaxation of the stresses. Thus, the value of compressive residual stress was optimized at the pulse density of 2500 pulses/cm^2.

(2) The amount surface ablated goes on increasing as we increase the pulse density. Therefore, the surface roughness was found to increase linearly with increasing pulse density. The surface roughness profile (Rz) of the unpeened specimen was increased by 46% after treating it with 2500 pulses/cm^2.

(3) After the specimen had been treated with low energy LSPwC process, the wettability of the material was found to have decreased. This is because contact angle of the specimen went from hydrophilic (34.24°) to hydrophobic (95.75°). The rise in the contact angle can be accounted to the increased surface roughness and the altered surface free energy. Nonetheless, this effect is highly desirable for enhancing pitting corrosion resistance as, as it leads to less water/ austenitic stainless steel contact, globally over the material.

(4) From the XRD graph, it can be said that both austenitic and martensitic phases were present in the microstructure created after solution annealing and water quenching. The high amount of compressive residual stress was generated after the LSPwC process. There was the beginning of a martensitic transformation in the specimen which was evident from the shift in γ-phase at around 43˚. From the difference in the relative intensities of the two peaks at 96°, it is evident that the martensite is forming as a result of deformation induced by the LSP process. There was a shift towards higher 2θ angles after the LSPwC process. However, there is no evidence of the martensitic transformation being complete.

(5) The optical microstructure and transmission electron microscopic images revealed deformation induced microstructural refinement features such as multidirectional mechanical twinning, dislocations lines, micro shear cells and stacking faults. These mechanical twins were found in near (50 microns) as well as subsurface regions in the cross section of LSPwC specimens. Grain refinement is clearly observed from transmission electron microscopic results. In austenitic stainless steels, a major way to deal with severe plastic deformation is deformation twinning. Therefore, from HR-XRD, TEM and Optical microstructure result it can be said that a trend is observed towards martensitic transformation. This is supported by the formation of deformation twins - the first step towards martensite transformation.

(6) The average hardness value of the laser shock peened specimens was found to be increased by 28% than the as-received specimens. This work hardening effect is on account of the major plastic deformation produced amid LSPwC process.

(7) No considerable change is witnessed in corrosion potential (Ecorr) and corrosion current density (Icorr) for LSPwC sample compared to the unpeened sample (Ecorr). The pitting potential after the LSPwC treatment was found to have increased from 1225 mV (unpeened) to 1450 mV. This was mainly due to CRS instigated in the specimen and the grain refinement. The corrosion pits were less prominent in the LSPwC specimen than the unpeened specimen. The hydrophobic transformation after the LSPwC process increased the pitting resistance. Increased pitting resistance could able to delay the crack initiation and propagation, and it helps to extend the fatigue life of the component.

(8) The metals which are used in nuclear reactors have to withstand the bombardment of nuclear particles in an aqueous and high-temperature environment. By LSPwC treating these materials their endurance against corrosion and radiation induced degradation processes can be enhanced. The improved hydrophobic nature after LSPwC can significantly support to improve the cell adhesion and wettability characteristics of the austenitic stainless steel for the biomedical implant applications.

Acknowledgement

The authors would like to thank VIT management for providing the incessant facilities and support.

References

[1] Lo, Kin Ho, Chan Hung Shek, and J. K. L. Lai. "Recent developments in stainless steels." *Materials Science and Engineering: R: Reports* 65.4 (2009): 39-104.

[2] Lu, Qiaofeng, Qing Su, Fei Wang, Chenfei Zhang, Yongfeng Lu, Michael Nastasi, and Bai Cui. "Influence of laser shock peening on irradiation defects in austenitic stainless steels." *Journal of Nuclear Materials* (2017).

[3] Zinkle, Steven J., and Jeremy T. Busby. "Structural materials for fission & fusion energy." *Materials Today* 12, no. 11 (2009): 12-19.

[4] Yvon, P., and F. Carré. "Structural materials challenges for advanced reactor systems." *Journal of Nuclear Materials* 385, no. 2 (2009): 217-222.

[5] Zinkle, Steven J., and G. S. Was. "Materials challenges in nuclear energy." *Acta Materialia* 61, no. 3 (2013): 735-758.

[6] Sano, Yuji, Minoru Obata, Tatsuya Kubo, Naruhiko Mukai, Masaki Yoda, Kiyotaka Masaki, and Yasuo Ochi. "Retardation of crack initiation and growth in austenitic stainless steels by laser peening without protective coating." *Materials Science and Engineering: A* 417, no. 1 (2006): 334-340.

[7] Kalainathan, S., S. Sathyajith, and S. Swaroop. "Effect of laser shot peening without coating on the surface properties and corrosion behavior of 316L steel." *Optics and Lasers in Engineering* 50, no. 12 (2012): 1740-1745.

[8] Peyre, P., X. Scherpereel, L. Berthe, C. Carboni, R. Fabbro, G. Beranger, and C. Lemaitre. "Surface modifications induced in 316L steel by laser peening and shot-peening. Influence on pitting corrosion resistance." *Materials Science and Engineering: A* 280, no. 2 (2000): 294-302

[9] Lu, J. Z., K. Y. Luo, Y. K. Zhang, G. F. Sun, Y. Y. Gu, J. Z. Zhou, X. D. Ren *et al*. "Grain refinement mechanism of multiple laser shock processing impacts on 304 stainless steel." *Acta Materialia* 58, no. 16 (2010): 5354-5362.

[10] Luo, K. Y., J. Z. Lu, Y. K. Zhang, J. Z. Zhou, L. F. Zhang, F. Z. Dai, L. Zhang, J. W. Zhong, and C. Y. Cui. "Effects of laser shock processing on mechanical properties and micro-structure of 304 austenitic stainless steel." *Materials Science and Engineering: A* 528, no. 13 (2011): 4783-4788

[11] Zhang, H. W., Z. K. Hei, Gang Liu, J. Lu, and K. Lu. "Formation of nanostructured surface layer on AISI 304 stainless steel by means of surface mechanical attrition treatment." *Acta materialia* 51, no. 7 (2003): 1871-1881.

[12] Montross, Charles S., Tao Wei, Lin Ye, Graham Clark, and Yiu-Wing Mai. "Laser shock processing and its effects on microstructure and properties of metal alloys: a review." *International Journal of Fatigue* 24, no. 10 (2002): 1021-1036.

[13] Dai, Fengze, Jianzhong Zhou, Jinzhong Lu, and Xinmin Luo. "A technique to decrease surface roughness in overlapping laser shock peening." *Applied Surface Science* 370 (2016): 501-507.

[14] Azhari, A., Christian Schindler, K. Hilbert, C. Godard, and Eberhard Kerscher. "Influence of waterjet peening and smoothing on the material surface and properties of stainless steel 304." *Surface and Coatings Technology* 258 (2014): 1176-1182.

[15] Zhang, Wenquan, Jinzhong Lu, and Kaiyu Luo. "Residual stress distribution and microstructure at a laser spot of AISI 304 stainless steel subjected to different laser shock peening impacts." *Metals* 6, no. 1 (2015): 6.

[16] Kalainathan, S., and S. Prabhakaran. "Recent development and future perspectives of low energy laser shock peening." *Optics & Laser Technology* 81 (2016): 137-144.

[17] Gujba, Abdullahi K., and Mamoun Medraj. "Laser peening process and its impact on materials properties in comparison with shot peening and ultrasonic impact peening." *Materials* 7, no. 12 (2014): 7925-7974.

[18] Sano, Yuji, Koichi Akita, Kiyotaka Masaki, Yasuo Ochi, Igor Altenberger, and Berthold Scholtes. "Laser peening without coating as a surface enhancement technology." *Pulse* 100, no. 40 (2006): 250mJ

[19] Zhang, L., Y. K. Zhang, J. Z. Lu, F. Z. Dai, A. X. Feng, K. Y. Luo, J. S. Zhong, Q. W. Wang, M. Luo, and H. Qi. "Effects of laser shock processing on electrochemical corrosion resistance of 304 stainless steel weldments after cavitation erosion." *Corrosion Science* 66 (2013): 5-13.

[20] Miwa, Masashi, Akira Nakajima, Akira Fujishima, Kazuhito Hashimoto, and Toshiya Watanabe. "Effects of the surface roughness on sliding angles of water droplets on superhydrophobic surfaces." *Langmuir* 16, no. 13 (2000): 5754-5760.

[21] Pratik Shukla, Jonathan Lawrence, and Yu Zhang. "Understanding laser beam brightness: A review and new prospective in material processing." *Optics & Laser Technology* 75 (2015): 40-51.

[22] Ramkumar, K. Devendranath, P. Siva Goutham Kumar, V. Radha Krishna, Aditya Chandrasekhar, Sidharth Dev, Winston Sunny Abraham, S. Prabhakaran, S. Kalainathan, and R. Sridhar. "Influence of laser peening on the tensile strength and impact toughness of dissimilar

welds of Inconel 625 and UNS S32205." *Materials Science and Engineering: A* 676 (2016): 88-99.

[23] Prabhakaran, S., and S. Kalainathan. "Compound technology of manufacturing and multiple laser peening on microstructure and fatigue life of dual-phase spring steel." *Materials Science and Engineering: A* 674 (2016): 634-645.

[24] Trdan, Uroš, Matej Hočevar, and Peter Gregorčič. "Transition from superhydrophilic to superhydrophobic state of laser textured stainless steel surface and its effect on corrosion resistance." *Corrosion Science* (2017). DOI:

[25] Sathyajith, S., S. Kalainathan, and S. Swaroop. "Laser peening without coating on aluminum alloy Al-6061-T6 using low energy Nd: YAG laser." *Optics & Laser Technology* 45 (2013): 389-394.

[26] Cullity BD. Elements of X-Ray Diffraction. 2nd ed.Addison-Wesley Inc; 1978.

[27] Patel, Divyansh, V. K. Jain, and J. Ramkumar. "Surface Texturing for Inducing Hydrophobicity." www.iitk.ac.in/directions/Directions_2015_01/surface_texturing.pdf

[28] Bagherifard, Sara, Ramin Ghelichi, Ali Khademhosseini, and Mario Guagliano. "Cell response to nanocrystallized metallic substrates obtained through severe plastic deformation." *ACS applied materials & interfaces* 6, no. 11 (2014): 7963-7985.

[29] Thangaraj, Balusamy, Sankara Narayanan TS Nellaiappan, Ravichandran Kulandaivelu, Min Ho Lee, and Toshiyasu Nishimura. "A facile method to modify the characteristics and corrosion behavior of 304 stainless steel by surface nanostructuring toward biomedical applications." *ACS applied materials & interfaces* 7, no. 32 (2015): 17731-17747.

[30]http://www.biolinscientific.com/zafepress.php?url=%2Fpdf%2FAttension%2FTheory%20Notes%2FAT_TN_7_roughness.pdf

[31] Hao, L., J. Lawrence, Y. F. Phua, K. S. Chian, G. C. Lim, and H. Y. Zheng. "Enhanced human osteoblast cell adhesion and proliferation on 316 LS stainless steel by means of CO2 laser surface treatment." *Journal of Biomedical Materials Research Part B: Applied Biomaterials* 73, no. 1 (2005): 148-156.

[32] Razi, Sepehr, Khosro Madanipour, and Mahmoud Mollabashi. "Improving the hydrophilicity of metallic surfaces by nanosecond pulsed laser surface modification." *Journal of Laser Applications* 27, no. 4 (2015): 042006.

[33] Hao, L., and J. Lawrence. "CO2 laser modification of the wettability characteristics of a magnesia partially stabilized zirconia bioceramic." *Journal of Physics D: Applied Physics* 36, no. 11 (2003): 1292.

[34] Caralapatti, Vinodh Krishna, and Sivakumar Narayanswamy. "Analyzing the effect of high repetition laser shock peening on dynamic corrosion rate of magnesium." *Optics & Laser Technology* 93 (2017): 165-174.

[35] Dryzek, E., M. Sarnek, and M. Wróbel. "Reverse transformation of deformation-induced martensite in austenitic stainless steel studied by positron annihilation." *Journal of Materials Science* 49, no. 24 (2014): 8449-8458.

[36] Prabhakaran, S., and S. Kalainathan. "Warm laser shock peening without coating induced phase transformations and pinning effect on fatigue life of low-alloy steel." *Materials & Design* 107 (2016): 98-107.

[37] Aniket Kulkarni, Siddarth Chettri, S. Prabhakaran, and S. Kalainathan. "Effect of laser shock peening without coating on surface morphology and mechanical properties of nickel-200." *Mechanics, Materials Science & Engineering MMSE Journal, Open Access* 9 (2017).

[38] Bahl, Sumit, Satyam Suwas, Tamas Ungar, and Kaushik Chatterjee. "Elucidating microstructural evolution and strengthening mechanisms in nanocrystalline surface induced by surface mechanical attrition treatment of stainless steel." *Acta Materialia* 122 (2017): 138-151.

[39] De, Amar K., David C. Murdock, Martin C. Mataya, John G. Speer, and David K. Matlock. "Quantitative measurement of deformation-induced martensite in 304 stainless steel by X-ray diffraction." *Scripta Materialia* 50, no. 12 (2004): 1445-1449.

[40] Mordyuk, B. N., Yu V. Milman, M. O. Iefimov, G. I. Prokopenko, V. V. Silberschmidt, M. I. Danylenko, and A. V. Kotko. "Characterization of ultrasonically peened and laser-shock peened surface layers of AISI 321 stainless steel." *Surface and coatings technology* 202, no. 19 (2008): 4875-4883.

[41] Zhou, Liucheng, Weifeng He, Sihai Luo, Changbai Long, Cheng Wang, Xiangfan Nie, Guangyu He, XiaoJun Shen, and Yinghong Li. "Laser shock peening induced surface nanocrystallization and martensite transformation in austenitic stainless steel." *Journal of Alloys and Compounds* 655 (2016): 66-70.

[42] Chen, A. Y., H. H. Ruan, J. Wang, H. L. Chan, Q. Wang, Q. Li, *Acta materialia* 59, no. 9 (2011): 3697-3709.and Jian Lu. "The influence of strain rate on the microstructure trtion of 304 stainless steel."

[43] Ye, Chang, Abhishek Telang, Amrinder S. Gill, Sergey Suslov, Yaakov Idell, Kai Zweiacker, Jörg MK Wiezorek *et al*. "Gradient nanostructure and residual stresses induced by

Ultrasonic Nano-crystal Surface Modification in 304 austenitic stainless steel for high strength and high ductility." *Materials Science and Engineering: A* 613 (2014): 274-288.

[44] Chen, A. Y., H. H. Ruan, J. B. Zhang, X. R. Liu, and Jian Lu. "Introducing a hierarchical structure for fabrication of a high performance steel." *Materials chemistry and physics* 129, no. 3 (2011): 1096-1103.

[45] Ye, Chang, Sergey Suslov, Dong Lin, and Gary J. Cheng. "Deformation-induced martensite and nanotwins by cryogenic laser shock peening of AISI 304 stainless steel and the effects on mechanical properties." *Philosophical Magazine* 92, no. 11 (2012): 1369-1389.

[46] Balusamy, T., TSN Sankara Narayanan, K. Ravichandran, Il Song Park, and Min Ho Lee. "Influence of surface mechanical attrition treatment (SMAT) on the corrosion behaviour of AISI 304 stainless steel." *Corrosion Science* 74 (2013): 332-344.

[47] Hong, T., and M. Nagumo. "Effect of surface roughness on early stages of pitting corrosion of type 301 stainless steel." *Corrosion science* 39, no. 9 (1997): 1665-1672.

[48] Ralston, K. D., and N. Birbilis. "Effect of grain size on corrosion: a review." *Corrosion* 66, no. 7 (2010): 075005-075005.

[49] Ralston, K. D., D. Fabijanic, and N. Birbilis. "Effect of grain size on corrosion of high purity aluminium." *Electrochimica Acta* 56, no. 4 (2011): 1729-1736.

[50] Lee, Han-sang, Doo-soo Kim, Jine-sung Jung, Young-shik Pyoun, and Keesam Shin. "Influence of peening on the corrosion properties of AISI 304 stainless steel." *Corrosion science* 51, no. 12 (2009): 2826-2830.

[51] Lu, J. Z., H. Qi, K. Y. Luo, M. Luo, and X. N. Cheng. "Corrosion behaviour of AISI 304 stainless steel subjected to massive laser shock peening impacts with different pulse energies." *Corrosion Science* 80 (2014): 53-59.

[52] Peyre, Patrice, C. Carboni, P. Forget, G. Beranger, C. Lemaitre, and D. Stuart. "Influence of thermal and mechanical surface modifications induced by laser shock processing on the initiation of corrosion pits in 316L stainless steel." *Journal of Materials Science* 42, no. 16 (2007): 6866-6877.

[53] Rokhlin, S. I., J-Y. Kim, H. Nagy, and B. Zoofan. "Effect of pitting corrosion on fatigue crack initiation and fatigue life." *Engineering Fracture Mechanics* 62, no. 4 (1999): 425-444.